JGR Atmospheres

RESEARCH ARTICLE
10.1029/2021JD035305

Special Section:
Advances in scaling and modeling of land-atmosphere interactions

The Effect of Land Use Classification on the Gas-Phase and Particle Composition of the Troposphere: Tree Species Versus Forest Type Information

M. L. Luttkus[1], E. H. Hoffmann[2], L. Poulain[2], A. Tilgner[2], and R. Wolke[1]

[1]Department Modeling of Atmospheric Processes, Leibniz Institute for Tropospheric Research (TROPOS), Leipzig, Germany, [2]Atmospheric Chemistry Department, Leibniz Institute for Tropospheric Research (TROPOS), Leipzig, Germany

Key Points:

- Detail of land use data sets crucial for biogenic volatile organic compound emission strength and composition
- Composition and concentration variation of these organic compounds induce changes in regional air quality predictions
- Detailed land use information, extended organic matter treatment, and high-resolution simulations are mandatory for air quality assessments

Supporting Information:

Supporting Information may be found in the online version of this article.

Correspondence to:

M. L. Luttkus,
luttkus@tropos.de

Citation:

Luttkus, M. L., Hoffmann, E. H., Poulain, L., Tilgner, A., & Wolke, R. (2022). The effect of land use classification on the gas-phase and particle composition of the troposphere: Tree species versus forest type information. *Journal of Geophysical Research: Atmospheres*, *127*, e2021JD035305. https://doi.org/10.1029/2021JD035305

Received 10 JUN 2021
Accepted 6 MAR 2022

Abstract Relationships between vegetation and air quality are intricate and still not fully understood. For regional air quality assessments, a better understanding of the diverse feedback mechanisms is crucial. The present article investigates the impact of land use data set detailedness on air quality predictions. Therefore, two different land use data sets were applied for simulations with COSMO-MUSCAT for Germany in May 2014. One data set includes detailed information about tree species while the second one obtains generalized widely applied land use classes including mixed and coniferous forests. Moreover, we examined the role of agricultural NO soil emissions, agricultural biomass density enhancements, and model resolution. For a more comprehensive implementation of the secondary organic aerosol (SOA) formation, the SOA module was extended considering additional biogenic volatile organic compound (BVOC) precursor groups from isoprene, α-pinene, limonene, and sesquiterpene oxidations. The model studies showed substantial differences in BVOC emission patterns between the two land use data sets. The application of detailed tree species information leads to complex BVOC emission patterns with high emission spots. In contrast, coarser forest information lead to standardized comprehensive emissions which result in 50% higher BVOC emissions. These differences affect both the atmospheric oxidizing potential and the production rates of SOA precursors. Land use induced regional differences (tree species minus forest information) in NO_x (±2.5%), ozone (−2.5%), OH (±50%), NO_3 radical (+70%) concentrations, and SOA (−60%) mass are modeled. Overall, the simulations demonstrate that detailed land use information, extended organic chemistry treatment, and high spatial resolution are mandatory for air quality assessments.

Plain Language Summary Trees are associated with being the lungs of the atmosphere as they filter out harmful substances from the air, they store CO_2, and produce oxygen via photosynthesis. Other by-products of photosynthesis are biogenic volatile organic compounds (BVOCs). BVOCs are chemical substances with a high vapor pressure already at room temperatures, so they quickly evaporate from the leaves into the surrounding air and are responsible for the characteristic forest smell. The amount and composition of BVOC emissions strongly depend on the tree species. Every plant has its own distinct emission properties. The chemical degradation of BVOCs impacts the chemical composition of the troposphere and is connected to ground level ozone production and the formation of secondary organic aerosols (SOA), contributing substantially to particulate matter (PM). On a global scale, standardized BVOC emission information on forest levels are often used, but for regional air quality assessments detailed plant specific information is crucial, but still often lacking. Therefore, two different land use data sets were applied in the present study to investigate the impact of standardized forest versus detailed tree-species information for Germany in May 2014. The study reveals changes in NO_x (±2.5%), ozone (−2.5%), OH (±50%), NO_3 radical (+70%), and SOA (−60%) concentrations.

1. Introduction

Tree planting programs are a key feature for climate change adaptation and mitigation strategies, as they have a large CO_2 storage potential (Bastin et al., 2019) and lower the ambient air temperature in dense urban areas, thereby reducing the urban head island effect (Schubert & Grossman-Clarke, 2013). Plants emit a complex mixture of highly reactive biogenic volatile organic compounds (BVOCs), such as isoprene, monoterpenes, sesquiterpenes, and other oxygenated VOCs (Atkinson & Arey, 2003). BVOCs are quickly oxidized by OH and NO_3 radicals as well as ozone (Atkinson, 2000; Atkinson & Arey, 2003) and thus influence the oxidizing potential of the

troposphere. The effects of BVOCs on air quality are much more complex and could have both a positive or negative impact (Fitzky et al., 2019; Popkin, 2019). The oxidation of BVOCs regardless of the oxidant can lower their volatility, which enables them to condense onto existing aerosol particles (Odum et al., 1996; Pankow, 1994) or even drive new particle formation (Ehn et al., 2014; Held et al., 2004; Jokinen et al., 2015; Lehtipalo et al., 2018; Riccobono et al., 2014). These two processes result in secondary organic aerosol (SOA) formation contributing to particulate matter (PM), which describes the total aerosol particle mass concentration and is grouped by its aerodynamic diameter (in μm) into PM_1, $PM_{2.5}$, and PM_{10} (von Schneidemesser et al., 2015).

Thus, BVOCs can impair air quality by influencing NO_x, ozone, and PM concentrations. So, they can have negative or eventually positive impacts on human health and ecosystems. Unfortunately, BVOC emission estimates bear huge uncertainties (Guenther et al., 2012; von Schneidemesser et al., 2015). BVOC emission models are sensitive to input parameters, such as meteorological conditions (temperature, solar radiation, etc.) and land use cover information (leaf area index LAI, plant functional type, and emission factors). Due to changes in these driving model parameters significant differences in global BVOC emission estimates can be found. Different setups of the widely used global framework MEGAN, the Model of Emissions of Gases and Aerosols from Nature, generate global isoprene emission values ranging from 350 to 800 Tg yr^{-1} (Guenther et al., 2012). For Europe, a detailed land use data set was published in 2001 containing about 116 tree species (Köble & Seufert, 2001), which is the basis for a comprehensive tree species-specific BVOC emission inventory (Karl, Guenther et al., 2009; Oderbolz et al., 2013; Steinbrecher et al., 2009). The emission algorithms within are based on Guenther et al. (1993) and Guenther (1997) and are therefore based on the same fundamentals as MEGAN. As BVOC emission itself is already highly uncertain, their simplified chemical degradation and approximated SOA forming potential makes climate and air quality assessments challenging. Global SOA budget estimates are still highly uncertain ranging from 12 to 1,820 Tg yr^{-1} (von Schneidemesser et al., 2015).

BVOC emission strengths and compositions are quite distinct between different tree species (Karl, Guenther et al., 2009; Steinbrecher et al., 2009) leading to varying air quality impacts. Additional land use induced effects on air quality are caused by changes in the meteorological fields primarily related to LU changes (urbanization, renaturation, deforestation, management, etc.) due to climate change or human activities (De Meij et al., 2015; De Meij & Vinuesa, 2014; Findell et al., 2017; García-García et al., 2020; Miralles et al., 2019; Seneviratne et al., 2010). Prescribed LU characteristics, such as the LAI, plant cover, root depth, and LU specific roughness length affect all surface fluxes (emissions, radiation, momentum, sensible, and latent heat) leading to changes in wind speed, temperature, relative humidity, and the boundary layer height pending on the land surface model used (for COSMO the land surface model is TERRA, e.g., Doms et al., 2013, 2018). Furthermore, the handling of the flux calculation affects the model performance. Two approaches are possible: (a) the dominant/bulk and (b) the mosaic approach. While the dominant/bulk approach only considers the dominant LU or bulk (weighted average) LU quantities, the mosaic approach considers individual contributions of all LU categories within the grid cell, which makes this approach less sensitive to spatial resolution (Li et al., 2013). Additionally, the deposition is linked to the LU classification (Schlünzen & Pahl, 1992; Simpson et al., 2012; Zhang et al., 2003).

In order to address climate mitigation and adaptation strategies as well as air quality assessments, more detailed knowledge of tree species-specific quantities are needed as currently most of the vegetation impacts are based on plant functional types. In the present article, we investigate the impact of LU classification detailedness on BVOC emissions by using two different LU data sets. While one data set contains detailed information about 138 LU classes (138_LU) including 116 tree species, the other one consists of 10 LU classes including only 2 simplified forest categories: mixed and coniferous forest (10_LU). Here, the effect of a reduction toward the forest level not only on BVOC emissions but also on the atmospheric oxidizing potential as well as air quality in terms of OH, NO_3, ozone, NO_x, and SOA concentrations is investigated with the model system COSMO-MUSCAT (see Section 2.1) for Germany in May 2014.

To further extent the representation of BVOCs in the chemical mechanism, reactions for sesquiterpene are implemented into the applied chemistry mechanism RACM (Stockwell et al., 1997). Furthermore, SOA products from monoterpenes + NO_3 reactions as well as isoprene and sesquiterpenes are added to the SOA module SORGAM (Schell et al., 2001). Several simulations were carried out for different scenarios and were compared with measurements from the field site Melpitz.

2. Model Setup and Description of the Measurement Site Melpitz

2.1. The Model System COSMO-MUSCAT

The MUltiScale Chemistry Aerosol Transport model MUSCAT is a state-of-the-art chemical transport model developed at the Leibniz Institute for Tropospheric Research (TROPOS). MUSCAT allows the use of several modules for emissions, chemistry, aerosol formation, and dynamics (Wolke et al., 2004, 2012; https://www.tropos.de/en/research/projects-infrastructures-technology/technology-at-tropos/numerical-modeling/cosmo-muscat). COSMO (version 5.05) is the numerical weather prediction model of the German weather service DWD (Schättler et al., 2018) and is online coupled to MUSCAT and works as the meteorological driver. The good performance of COSMO-MUSCAT regarding air quality simulations has been validated and confirmed by model intercomparison studies, for example, the Air Quality evaluation International Initiative AQMEII (Im et al., 2014a, 2014b; Solazzo, Bianconi, Pirovano et al., 2012; Solazzo, Bianconi, Vautard et al., 2012). The studied model area is Germany (N2; orange area in Figure S1 in Supporting Information S1). To generate the initial boundary conditions for the model domain N2 a European model run (N1; brown area in Figure S1 in Supporting Information S1) has been performed first. The European run itself uses 3 hr ECMWF-IFS CAMS boundary and initial data for aerosols (sea salt, dust, organic matter, black carbon, and sulfate), gas-phase concentrations (NO_2, CO, SO_2, HCHO, H_2O_2, O_3, NO, HNO_3, OH radicals, PAN, isoprene, methane, methanol, ethene, ethane, ethanol, and propane), and temperature data. The resolution of the model domain N1 is 28 km × 28 km and for N2 7 km × 7 km and roughly 22 km height for COSMO for both domains while N1 contains 40 and N2 50 levels; 10 and 12 levels being within the first 1,000 m, respectively, with the first level at 20 m. MUSCAT is restricted to 8 km height. MUSCAT uses a multi-block approach which allows different horizontal resolutions by defining multiple blocks within the grid (Knoth & Wolke, 1998a, 1998b; Wolke & Knoth, 2000). An implicit-explicit (IMEX) time integration scheme is used in MUSCAT (Knoth & Wolke, 1998a, 1998b; Wolke & Knoth, 2000). The explicit time step is based on the slow process of horizontal advection and the corresponding CFL-criterion, while the implicit time steps take into account the faster processes of vertical exchange and chemical transformation splitting one explicit time step into several implicit ones separately for every block.

2.2. Land Use Data Sets

Two simulations with different LU data sets, the 138_LU (Köble & Seufert, 2001) and 10_LU are carried out to test the sensitivity of the model toward tree species versus forest level information. The 138_LU contains 116 tree classes, 11 agricultural land use types, and additional vegetated (wetlands, grassland, green urban area, etc.) and non-vegetated land use categories (water bodies, artificial surfaces, etc.). To study the effect of more generalized land use types, commonly used for global model estimates, the 138 land use classes have been transformed into the following 10 classes: water, mudflats, sand, mixed land use (mainly agriculture), meadows, heath, bushes, mixed forest (broadleaved trees), conifer forest (coniferous trees), and urban area. In this way, the contribution of trees and forests in a grid cell are kept equal. These 10 classes have been used in COSMO-MUSCAT simulations for this model domain so far and are linked to the implemented deposition scheme (Schlünzen & Katzfey, 2003; Schlünzen & Pahl, 1992). The simulations using the generalized land use will have the prefix 10_LU. The data set from Köble and Seufert (2001) has a resolution of 1 km × 1 km. For the simulations, the data set has been resampled onto the model grid giving the percentage distribution of all land use classes for each grid cell (Figure 1).

The distribution of the different LU categories is crucial for the BVOC emission patterns which subsequently affect the spatial and temporal distribution of oxidizing agents and reaction products. In preparation for the model results the most common vegetation types of both LU data sets are addressed first. The Figures 1a, 1e,and 1i belong to the 10_LU data set, Figure 1d is part of both data sets and the remaining panels show the distribution for the 138_LU. If more than one tree species is present in the model domain for the 138_LU they are grouped together and presented on a genus level. The first row depicts agricultural LU categories, the second row deciduous and the third-row coniferous tree classes. Comparing the general LU class mixed land use (Figure 1a) with Figure 1b reveals non-irrigated arable land as the dominating agricultural LU category and is present throughout the whole domain with a large proportion from the Netherlands through Germany with a maximum in the center till the Czech Republic which is here denoted as the NW-SE agricultural band (see Figure S1 in Supporting Information S1). The LU class representing agricultural and natural vegetation (Figure 1c) is more pronounced in the Czech Republic, in Poland (line parallel to the Baltic Sea) and a spot in the Netherlands close to the German

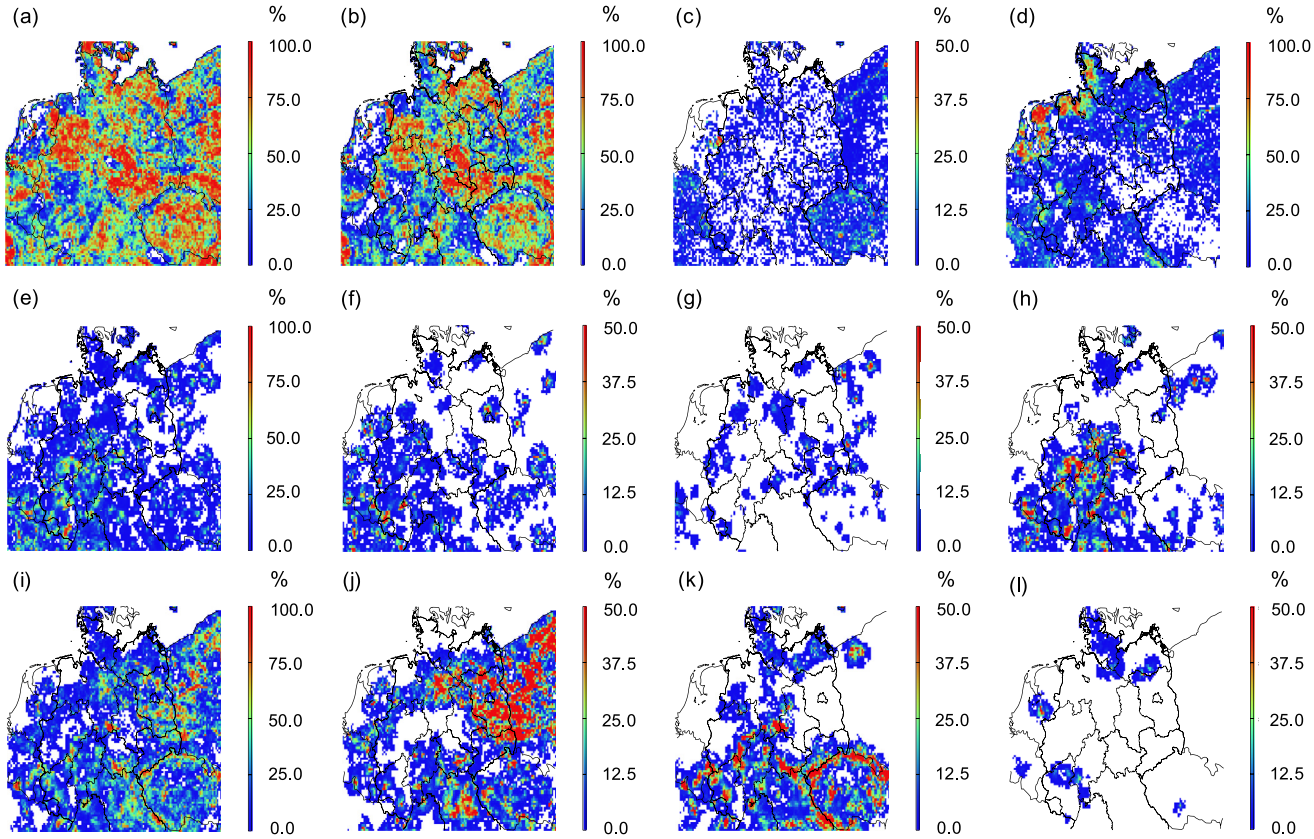

Figure 1. Relative distribution of (a) mixed land use, (b) non-irrigated arable land, (c) agricultural and natural vegetation, (d) meadow, (e) mixed forest, (f) oak species, (g) birch species, (h) common beech, (i) conifer forest, (j) pine species, (k) spruce species, and (l) Douglas fir showing values greater than 0.004%.

border. Meadows (Figure 1d) are dominating along the coast of the North Sea. The agricultural LU categories are of importance for the sensitivity studies presented in Section 3.4 and 3.5.

All deciduous trees are grouped into the forest category mixed forest (Figure 1e) for the 10_LU and occur more frequent in the middle and south west of the domain. For 138_LU oak (Figure 1f: *Quercus robur*, *Quercus petraea*, and *Quercus rubra*) and birch (Figure 1g: *Betula pubescens* and *Betula pendula*) species as well as common beech (Figure 1h) are the most important broad-leafed tree species for Germany. If more than one tree species is present the predominant one is underlined. Common beech is the most frequent occurring broad-leafed tree species followed by oaks. Beech show higher ratios in the middle and south west of the domain, additional spots appear in northern Poland and Germany. Oaks are present in small rations throughout the whole domain but larger fractions occur around Berlin, a few spots in Poland and more frequent in the west of the domain. Smaller spots can be found for birch species in the whole domain with largest proportion in Poland.

The generalized LU category conifer forest (Figure 1i) sums up all the coniferous tree species and shows a higher percentage distribution in the east and south of the domain. When considering tree species, a clear separation between pine (Figure 1j: *Pinus sylvestris*, *Pinus nigra*, and *Pinus strobus*) and spruce (Figure 1k: *Picea abies* and *Picea sitchensis*) species is visible. Pine species dominate the north east (Brandenburg and Poland). They also reach around from Brandenburg to the Netherlands and along the German border until the Rhine and are frequently present in the south. Spruce species predominate the lower mountain range which is in the southern model domain and a few areas in the north for which the highest ratio is reached in north Poland. Douglas fir (Figure 1l) show only minor overall contribution but its huge BD (of 1,000 g m^{-2}) makes it an intriguing tree species when looking at the effects of BVOC emissions on air quality. Only a few spots are present in the north, west and one in the Czech Republic with the highest contribution in the Netherlands.

2.3. Emissions

For anthropogenic emissions, the MACC 2010 (Kuenen et al., 2014; Pouliot et al., 2015) inventory is applied for Europe. For Germany, data from the federal environmental agency (UBA) was made available using GRETA, the Gridding Emission Tool for ArcGIS (Schneider et al., 2016). BVOC emissions E_{sl} are parametrized according to Steinbrecher et al. (2009):

$$E_{sl} = A_l \times BD_l \times SEP_{sl} \times \gamma.$$

And uses information about the area A covered by a certain LU type (indicated by lower index *l*), biomass densities (BDs in g m^{-2}), plant species-specific standard emission potentials SEPs (µg g^{-1} h^{-1} at 30°C and photosynthesis-active radiation of 1,000 µmol m^{-2} s^{-1}) for varies BVOCs (indicated by lower index *s*) and a correction factor γ for seasonality, temperature, and light. A more detailed discussion of BVOC emissions parametrization and its constraints can be found in the supplement (Text S1 in Supporting Information S8). The product of BD with the SEP is called the standard emission factor. The following BVOC emissions are included: isoprene, 17 monoterpenes (α- and β-pinene, camphene, Δ^3-carene, sabinene, α-thujene, limonene, α- and γ-terpinene, α- and β-phellandrene, myrcene, trans- and cis-ocimene, linalool, *p*-cymene, and 1,8-cineol), sesquiterpene (β-caryophyllene), and oxygen containing BVOCs (OVOCs: methanol, acetone, ethanol, acetaldehyde, formaldehyde, formic acid, and acetic acid). Trees are supposed to emit sesquiterpenes while for other land use categories, such as agriculture and grass land it remains uncertain. Karl, Guenther et al. (2009) suggested sesquiterpene emissions for all LU categories including agriculture while Steinbrecher et al. (2009) only present sesquiterpene SEPs for trees but not for agricultural LU categories. Oderbolz et al. (2013) list 0 as SEP for agricultural sesquiterpene emission. Therefore, here crops are treated as non-sesquiterpene emitting and other land use categories (natural and urban vegetation, shrubs, and trees) are assigned 0.1 µg g^{-1} h^{-1}. Except for agriculture and a few tree species, all LU classes are assigned a sesquiterpene SEP of 0.1 µg g^{-1} h^{-1} (Karl, Guenther et al., 2009; Oderbolz et al., 2013; Steinbrecher et al., 2009).

2.4. Chemistry Mechanism

Even though a diverse monoterpene emission split is available, there are only a few monoterpenes represented even in near-explicit gas-phase chemistry mechanisms (e.g., MCMv3.3.1: α- and β-pinenes and limonene; http://mcm.york.ac.uk/home.htt). In this study, the widely used chemistry mechanism RACM-MIM2-ext (Karl et al., 2006; Stockwell et al., 1997) is used and extended with additional reactions for sesquiterpenes (Karl, Tsigaridis, Vignati, & Dentener, 2009). RACM-MIM2-ext only treats monoterpene in terms of α-pinene (API) and limonene (LIM) and thus the 17 monoterpenes given by Steinbrecher et al. (2009) have been grouped as follows: cyclic terpenes with one double bond (α- and β-pinenes, camphene, Δ^3-carene, sabinene, and α-thujene) are grouped into API and monoterpene with more than one double bond (limonene, α- and γ-terpinenes, α- and β-phellandrenes, myrcene, trans- and cis-ocimene, and linalool) are grouped into LIM with α-pinene and limonene still being the representative of this group. If in the following sections α-pinene and limonene are mentioned, they always refer to the API- and LIM clusters. *p*-Cymene, which is a biogenic aromatic compound (BARO), is treated as xylene and 1,8-cineol, which is a cyclic ether, is treated as RACM lumped group species HC8 (BHC8).

BVOCs impact both the production and degradation of radicals and photo oxidants. Therefore, a simplified description of the implemented VOC chemistry is given in the following, only showing reactions used in the chemistry mechanism RACM-MIM2-ext. A more complex VOC chemistry description can be found in Atkinson (2000) and Atkinson and Arey (2003). Photolysis parameters are taken from MCMv3.3.1. The photolysis of ozone generates excited oxygen $O(^1D)$ and ground-state oxygen $O(^3P)$ as well as molecular oxygen (R1a and R1b). $O(^1D)$ can collide with N_2 or O_2 (M) losing the excess energy and becoming $O(^3P)$ or reacts with water vapor generating two OH (R2, R3). The reaction of $O(^3P)$ with molecular oxygen reproduces the ozone molecule (R4).

$$O_3 + h\nu \rightarrow O(^1D) + O_2, \quad \text{(R1a)}$$

$$O_3 + h\nu \rightarrow O(^3P) + O_2, \quad \text{(R1b)}$$

$$O(^1D) + M \rightarrow O(^3P) + M, \quad \text{(R2)}$$

$$O(^1D) + H_2O \rightarrow OH + OH, \quad \text{(R3)}$$

$$O(^3P) + O_2 \xrightarrow{M} O_3 \quad \text{(R4)}$$

In the presence of NO_x ozone is quickly oxidized by NO (R5) producing NO_2 which gets photolyzed (R6) to NO and $O(^3P)$. Between these reaction sequence, a photostationary state is established (Leighton relationship).

$$O_3 + NO \rightarrow NO_2 + O_2, \quad \text{(R5)}$$

$$NO_2 + h\nu \rightarrow O(^3P) + NO. \quad \text{(R6)}$$

This equilibrium is disturbed by BVOC degradation processes through the production of intermediate BVOC products (R7), the organic peroxy radicals (RO_2). Instead of ozone, NO can also react with RO_2 to form NO_2 (R8). In addition, HO_2 is produced which can also react with NO to form NO_2 and OH (R9). Besides the reaction with NO, RO_2 radicals can react with other radicals: HO_2, methyl peroxy (MO_2), acetyl peroxy (ACO_3), NO_3, and self-reactions (not shown). Furthermore, oxidized BVOCs are produced from R7 and R8 and subsequent RO_2 oxidation processes so that R7 initializes SOA formation. Additional SOA initialization reactions of BVOC equivalent to R7 are the reaction with ozone or the nitrate radical (NO_3; both not shown).

$$VOC + OH \rightarrow RO_2, \quad \text{(R7)}$$

$$RO_2 + NO \rightarrow NO_2 + HO_2 + \text{products}, \quad \text{(R8)}$$

$$HO_2 + NO \rightarrow OH + NO_2. \quad \text{(R9)}$$

Nitrate radicals are produced by reactions of NO_2 with ozone (R10). During the day, NO_3 radicals are rapidly photolyzed (R11a and R11b), or quickly react with NO (R12). The reaction of OH radicals with NO_2 leads to the formation of nitric acid (HNO_3) and is a major daytime NO_x and HO_x (sum of OH and HO_2) loss processes (R13). During night, the formation of dinitrogen pentoxide (N_2O_5) from the reaction of NO_3 radicals with NO_2, which is a reversible process (R14), and its wet and dry deposition as well as aerosol uptake are important NO_x loss processes due to the hydrolysis into HNO_3. The production of nitrous acid (HONO) from OH radicals and NO (R15) is in photo equilibrium with HONO photolysis (R16).

$$NO_2 + O_3 \rightarrow NO_3 + O_2, \quad \text{(R10)}$$

$$NO_3 + h\nu \rightarrow NO_2 + O(^3P), \quad \text{(R11a)}$$

$$NO_3 + h\nu \rightarrow NO + O_2, \quad \text{(R11b)}$$

$$NO_3 + NO \rightarrow NO_2 + NO_2, \quad \text{(R12)}$$

$$OH + NO_2 \xrightarrow{M} HNO_3, \quad \text{(R13)}$$

$$NO_3 + NO_2 \xleftrightarrow{M} N_2O_5, \quad \text{(R14)}$$

$$OH + NO \rightarrow HONO, \quad \text{(R15)}$$

$$HONO + h\nu \rightarrow OH + NO. \quad \text{(R16)}$$

BVOCs can be quickly oxidized by ozone, OH, or NO_3 radicals (see lifetime Figures S42–S44 in Supporting Information S7; Atkinson, 2000; Atkinson & Arey, 2003; Oderbolz et al., 2013). OVOCs, *p*-cymene, and 1,8-cineol react preferably with OH radicals (Atkinson & Arey, 2003; Corchnoy & Atkinson, 1990; Oderbolz et al., 2013). Isoprene can react fast with OH radicals and somewhat slower with NO_3 radicals and O_3 (Atkinson & Arey, 2003; Oderbolz et al., 2013). Monoterpene groups API and LIM are oxidized by OH radicals during the day and rapidly by NO_3 radicals during night, reactions with O_3 can also occur throughout the day (Atkinson & Arey, 2003; Oderbolz et al., 2013). Degradation of sesquiterpenes is dominated by O_3 followed by NO_3 and OH radicals (Atkinson & Arey, 2003; Oderbolz et al., 2013). The volatility of anthropogenic (AVOC) and BVOCs drops with every chemical functionalization process enabling the oxidation products formed to condense onto

particles (Odum et al., 1996; Pankow, 1994) or initiate new particle formation (Ehn et al., 2014; Held et al., 2004; Jokinen et al., 2015; Lehtipalo et al., 2018; Riccobono et al., 2014) and thereby producing SOA. The SOA yield itself depends on the specific VOC oxidant reaction and the total available absorbing organic matter OM (Pankow, 1994). The initial reaction of sesquiterpenes with ozone followed by a second oxidation leads to a SOA yield of more than 100% (Hoffmann et al., 1997) making it the most efficient one followed by the reaction of monoterpenes and isoprene with NO_3, O_3, and OH, respectively.

2.5. Updated SOA Module

The formation of SOA is described by the 2-product approach SORGAM (Schell et al., 2001) which was implemented into RACM-MIM2-ext without changing the gas-phase chemistry mechanism. The original SORGAM module only includes SOA products for API and LIM from OH and ozone oxidation, as well as anthropogenic VOCs: aromatic precursors (toluene, xylene, and cresol), higher alkane (HC8), and higher alkenes (OLT and OLI). During the plant growing season and BVOC emission favoring meteorological conditions (warm temperatures and high solar radiation) SOA production is substantially underestimated mainly due to lacking BVOC SOA treatment (see Section 3.7). To improve the SOA formation model performance, SORGAM was updated by reactions for monoterpenes with NO_3 (Griffin et al., 1999), isoprene (Kroll et al., 2006; Ng et al., 2008), sesquiterpenes (Hoffmann et al., 1997; Karl, Tsigaridis, Vignati, & Dentener, 2009), and reaction pathways for highly oxidized multifunctional organic molecules HOMs (monoterpene: Berndt, Richters et al., 2016; Jokinen et al., 2015; sesquiterpenes: Richters et al., 2016; isoprene: Berndt, Herrmann, Sipilä, & Kulmala, 2016). The BVOC SOA products and corresponding reactions are summarized in Tables S1 and S2 in Supporting Information S1. For monoterpenes, the saturation vapor pressure (P^0) values from Schell et al. (2001) were used while the stoichiometric coefficients α_i were calculated with python3 from SOA yield measurements for β-pinene NO_3 radical reaction from Griffin et al. (1999) showing a correlation of 0.9963. Differences in α_i for API and LIM are due to different molar masses of the SOA products. The values for P^0 of isoprene are chosen in a way that the fit for OH as well as NO_3 radical reactions in combination with the corresponding α_i show good correlations with SOA experiments (see Figure S55 in Supporting Information S8; OH: Kroll et al., 2006; NO_3: Ng et al., 2008) while prioritizing the NO_3 radical reaction due to its higher SOA forming potential (0.906 and 0.998, respectively). For clear separation of biogenic and anthropogenic SOA sources as well as their oxidizing agents, all SOA products are addressed separately resulting in 38 different SOA products (see Table S1 in Supporting Information S1).

2.6. Melpitz

To test the SOA module update and compare the simulations with measurements, the time period May 2014 was chosen as during this month an intensive measurement campaign took place at the TROPOS field site Melpitz (see Section 3.7). The TROPOS research site Melpitz (51.54°N, 12.93°E, 86 m a.s.l) is a regional background station situated about 50 km to the Northeast of Leipzig in a glacial valley of the river Elbe. The research site Melpitz itself is on a flat meadow surrounded by agriculture (Spindler et al., 2013). The grid cell within COSMO-MUSCAT that includes Melpitz consists of 87.7% agriculture, 7.9% artificial surfaces, 2.6% pine forests, and 1.8% water bodies. Melpitz is integrated in EMEP (Co-operative program for monitoring and evaluation of the long-range transmission of air pollution in Europe), as well as the European scientific infrastructure ACTRIS (Aerosol, Clouds and Trace gases Research Infrastructure) and the German Ultrafine Aerosol Network (GUAN). For a basic overview of the physical and chemical aerosol characterization methods see for example, Birmili et al. (2008), Poulain et al. (2011), Poulain et al. (2014), Spindler et al. (2012), and Spindler et al. (2013).

3. Model Results

The influence of LU data set detailedness on air quality is addressed by difference plots of the average map plots during May 2014 for various scenarios between the detailed and the generalized LU data set focusing on BVOC emissions induced responses to tree species versus forest classifications. The differences between the two LU data sets are key to model simulation analysis and are therefore continuously shown, always comparing 138_LU with 10_LU (138_LU–10_LU), if not stated otherwise. The diversity of LU classes and their individual SEP and BD for the 138_LU strongly influences BVOC emission strengths, composition, and individual patterns. Note

that the tree species composition is crucial for the BVOC composition and therefore, the results of this regional analysis cannot directly be transferred to other regions with different tree populations. An overview of minimum, average, and maximum values of the different scenarios can be found in Table S3 in Supporting Information S1.

While analyzing the influence of detailed LU versus simplified forest information on BVOC emissions the link between certain tree species and corresponding low and/or high BVOC emissions as well as oxidants, BVOCs, and SOA concentration levels are investigated. Additionally, the impact of NO on these interdependencies are addressed by secondary agricultural NO soil emissions. For the same reason, agricultural BD is increased which affects the BVOC emission strengths. Next to these model sensitivity studies the model spatial and temporal resolution was refined as preliminary step for comparisons with measurements from Melpitz.

3.1. BVOC Emission Differences

The two LU data sets have a major impact on BVOC emissions and can cause drastic regional changes. For the 138_LU isoprene emission (Figure S2 in Supporting Information S2) is dominated by oaks (*Quercus robur*: SEF 22,400 μg m^{-2} h^{-1}; *Quercus petraea*: SEF 14,400 μg m^{-2} h^{-1}; *Quercus rubra*: SEF 11,200 μg m^{-2} h^{-1}). Additional sources are poplar (SEF 18,200 μg m^{-2} h^{-1}), maple (SEF 27 μg m^{-2} h^{-1}), Douglas fir (SEF 1,000 μg m^{-2} h^{-1}), robinia (SEF 3,600 μg m^{-2} h^{-1}), willow (SEF 11,160 μg m^{-2} h^{-1}), and elm trees (SEF 30 μg m^{-2} h^{-1}). Oak species, poplar, and willow have a higher SEF compared to the SEF of the generalized LU categories mixed (5,000 μg m^{-2} h^{-1}) and conifer forest (3,000 μg m^{-2} h^{-1}). As poplar and willow do not frequently occur or only in small proportions, high isoprene emission spots for the 138_LU are linked to oak species and are visible around Berlin, in Poland, and the western model domain with a maximum of 1,494.1 μg m^{-2} h^{-1} revealing quite distinct isoprene emission patterns. The 10_LU shows rather widespread emissions with a higher mean emission of 90.2 μg m^{-2} h^{-1} (177.9%) compared to 50.7 μg m^{-2} h^{-1} but a much lower maximum value of 474.7 μg m^{-2} h^{-1} (31.8%). Except for the tree species spots the difference between the LU data sets is always negative (Figure 2 and Figure S2 in Supporting Information S2).

Monoterpene emission is governed by coniferous species of pine and spruce trees (Figures 1j and 1k) and to some extend also by beech (*Fagus sylvatica*; Figure 1h). Table S4 in Supporting Information S1 includes values for BD, SEP, and SEF for the four monoterpene groups α-pinene, limonene, *p*-cymene, and 1,8-cineol for the LU classes *Picea abies*, *Pinus sylvestris*, *Fagus sylvatica*, coniferous, and mixed forest. The two forest categories include the standard monoterpene emission split. According to Steinbrecher et al. (2009), 32 tree species show an individual monoterpene emission split based on measurements including the two dominating conifers *Picea abies* and *Pinus sylvestris* as well as beech. The remaining tree species were assigned a default monoterpene split (API 71%, LIM 23%, BARO 4%, and BHC8 2%).

Picea abies predominates the lower mountain range of Germany while *Pinus sylvestris* is more frequent in the north east. The combination of SEF with the emission split results in similar but lower α-pinene emission for pine, spruce, and most deciduous trees. Beech has a significant higher SEF. These tree species induced differences in SEF compared to the standardized values cause alternating emission values in the middle and south west of the domain as well as northern Poland while the rest is negative (Figure 2 and Figure S3 in Supporting Information S2). Limonene emissions are lower throughout the whole model domain (Figure 2 and Figure S3 in Supporting Information S2) especially for pine forests. The main contributor to 1,8-cineol emission (Figure S4 in Supporting Information S2) is *Picea abies*, followed by birch trees and again a decrease for pine forests (Figure 2). *p*-Cymene are emitted by *Pinus nigra* and Douglas fir, which not frequently occur in the model domain. Therefore, *p*-cymene emission is highly overestimated (six times higher mean value; see Table S3 in Supporting Information S1) when using 10_LU (Figure S4 in Supporting Information S2). Note that the default monoterpene emission split is used for *Pinus nigra* and Douglas fir. Pending on the literature used, both could be treated as non *p*-cymene emitters or with low contribution to the monoterpene emission. Steinbrecher et al. (2009) reports a contribution of 4% for *p*-cymene while Geron et al. (2000) and Faiola et al. (2015) state a contribution of 0% and 1.7% for Douglas fir. *Pinus nigra* is identified as non *p*-cymene emitter (Geron et al., 2000; Harley et al., 2014) but small concentrations were detected in essential oils from needles, branches, and cones (Macchioni et al., 2003; Supuka et al., 1997).

Sesquiterpene (Figure S4 in Supporting Information S2) and OVOC (Figure S2 in Supporting Information S2) emissions are almost exclusively controlled by BD as most tree species have the same SEP (sesquiterpenes:

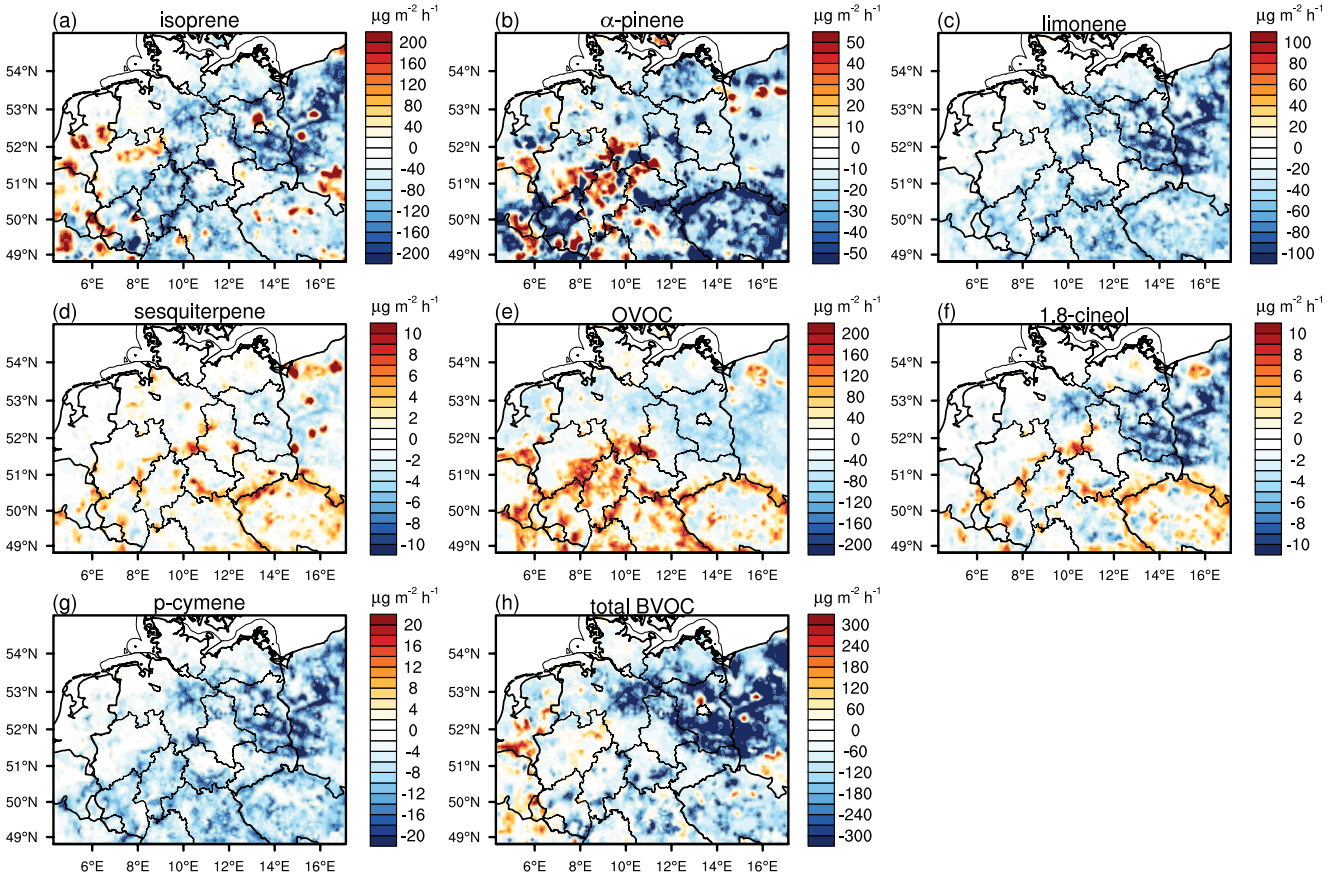

Figure 2. LU-induced changes of BVOC emissions presented in differential plots (138_LU–10_LU). The values present average values during May for (a) isoprene, (b) α-pinene, (c) limonene, (d) sesquiterpenes, (e) OVOCs, (f) 1,8-cineol, (g) *p*-cymene, and (h) total BVOC emission.

0.1 µg g^{-1} h^{-1}; OVOC: 2 µg g^{-1} h^{-1}). Exceptions are birch trees (SEP: 2 µg g^{-1} h^{-1}) for sesquiterpenes, and spruces (*Picea abies* 2.3 µg g^{-1} h^{-1}; *P. sitchensis*: 2.89 µg g^{-1} h^{-1}) as well as beeches (10 µg g^{-1} h^{-1}) for OVOCs. The smaller BD of pine trees generates lower and the higher BD of spruces higher OVOC and sesquiterpene emissions. Higher sesquiterpene emissions are also located in the southern model domain and Poland's birch and spruce forests (Figure S4 in Supporting Information S2). For OVOCs, higher emissions occur in the German lower mountain ranges and Poland's spruce and beech forests (Figure 2 and Figure S2 in Supporting Information S2). Higher OVOC emissions over the Netherlands are caused by a larger BD of the agricultural LU class complex cultivated patterns (distribution not shown) compared to the mixed LU class of 10_LU. As agricultural LU categories are treated as non-sesquiterpene emitting this is not evident in the sesquiterpene emission plot.

These results are in good agreement with Steinbrecher et al. (2009) and Oderbolz et al. (2013) which are both based on the LU data set from Köble and Seufert (2001). They present similar emission patterns but for time periods July 2000 and June 2006, respectively. The emissions are in the same range (0–350 kg km^{-1} $month^{-1}$), however, differences are related to different model systems, meteorological conditions, and time of the year. Unfortunately, these articles only focused on BVOC emissions.

The reduction to forest level information leads to 50% overestimated BVOC emissions (excluding OVOCs) compared to detailed trees species information influencing not only BVOC emission strengths but also the emission patterns and composition. Certain tree species emit higher amounts than their corresponding forest category resulting in BVOC emission spots: (a) oaks for isoprene, (b) birch and spruce for sesquiterpenes, (c) beech and spruce for OVOCs, (d) beech for α-pinene, and (e) spruce for 1,8-cineol. OVOC emissions show similar mean values for Germany independent of the LU (161.5 µg m^{-2} h^{-1} for 10_LU and 162.4 µg m^{-2} h^{-1} for 138_LU) but different spatial distributions: lower values in the north and higher values in the south for the 138_LU. Moreover,

as every single BVOC has its preferred oxidizing partner, their degradation strongly effects the distribution and concentration of their oxidants: ozone, OH, and NO_3 radicals.

3.2. Impacts on Predicted BVOC and Oxidants Concentration Levels

3.2.1. Modeled BVOC Concentration Patterns

The mean modeled BVOC concentration patterns are similar to the emissions mainly just with changed units and scales. Therefore, they are not described in detail here but are given for the sake of completeness in the supplement (see Figures S5–S11 in Supporting Information S2).

3.2.2. Link Between BVOC and Oxidant Concentrations

LU induced BVOC emission changes affect the tropospheric oxidants budget by consumption due to degradation as well as production processes. For OH and NO_3 radicals, the consumption dominates, always linking higher BVOC emissions with lower oxidant concentrations in the grid cell. For ozone, it is more complex due the overlaying consumption and production processes which are additionally linked to RO_2 and NO_x concentrations (mainly R1–R10). In order to examine certain pattern or possible interplays between BVOC concentrations and oxidants, not only difference plots but also temporal correlation analyses for the entire grid were performed to gain additional information. Temporal correlations for every single grid cell are calculated using the Pearson sample linear cross-correlation function for ground-level model concentration values. Instead of showing several time series for numerous spots of the model domain and calculating correlations individually, here the correlation between two time series of different concentrations in every single grid cell of the domain are summarized in correlation map plots (Figures S13, S14, S16, S17, S19, S20, S24, and S25 in Supporting Information S3 and S4). A few sets of time series with additional information for selected spots are given in the supplement (Figure S45–S52 in Supporting Information S7). However, the interpretation of correlations between BVOCs and other concentrations are intricate as the emission of BVOCs, their chemical degradation as well as oxidant production show either similar or opposing diurnal cycles. Furthermore, their distribution is additionally influenced by the meteorology. BVOC emissions are stimulated be temperature and solar radiation. Synthesis emission onset comes with radiation while pool emission might rise earlier if temperature already increases before sunrise. These enhanced morning emissions are followed by concentration increases. Atmospheric photolysis processes proceed at the same time producing ozone and thus initiate OH radical generation. If oxidant production becomes efficient, the BVOC depletion by chemical reaction with the oxidant compensates the BVOC emission and the BVOC concentration declines until photo-chemical oxidant production becomes inefficient. If BVOC emission progresses, they can accumulate again until in the case of synthesis emission their emission ceases. In this case, if chemical degradation progresses, the BVOC might become totally depleted. For pool emission, lower emissions will continuously provide BVOCs which leads to an accumulation during night if their oxidation is governed by OH radicals. In the case of NO_3 degradation pathways, the same as for the photolysis oxidants repeats. Until NO_3 production via R10 becomes sufficient, BVOCs accumulate. Afterward, BVOC depletion starts until the NO_3 becomes insufficient and an accumulation appears again until photolysis sets in.

3.2.2.1. OH

The OH mean concentration (Figure S12 in Supporting Information S2) is primarily linked to isoprene and second to OVOCs reducing OH radical concentration in high emission regions (Figure 2). The difference plots (Figure 2 and Figures S2, S5, and S12 in Supporting Information S2) are therefore inversely colored showing maximum values for isoprene and at the same location minimum values for OH and vice versa. Except for isoprene emission spots of oaks, isoprene concentration for 138_LU are low reaching nearly 100% reduction in forests predominantly consisting of pines and second spruce. Highest OH concentration rise is reached in non-isoprene emitting pine forests. The higher OVOC and low isoprene emissions (Figure 2) of spruce and beech trees diminish the OH concentration rise and reduce the contrast to the generalized forest categories in the southern model domain.

Main OH production occurs during the day via photochemistry therefore, only day-time values are considered (concentrations between 4 UTC and 18 UTC + 0:00, with the maximum at 12 UTC) for temporal correlations. Lifetime of BVOCs due to OH is in the range of 0.5 till 2.5 hr for API, LIM, ISO, and SQT (Figure S42 in Supporting Information S7). For isoprene, the 10_LU shows positive correlations (Figure S13 in Supporting Information S2) as OH production and isoprene emission have similar diurnal cycles and the moderate meteorological conditions

till mid of May inhibits an effective early morning rise for synthesis emissions like isoprene and hinder photosynthesis OH production. In the 138_LU correlation plot also negative values are present (Figure S14 in Supporting Information S2) at high isoprene emission spots of oaks. Here, the fast intensification of isoprene emission with the onset of solar radiation quickly increase isoprene concentration which is then compensated by OH production until it becomes insufficient and isoprene accumulates again (Figures S51 and S52 in in Supporting Information S7). Negative BVOC correlations are present where the early morning peak is followed by a decrease, which except for the isoprene emission spots is more likely for pool emissions (Figure S49 in in Supporting Information S7) in BVOC rich environments, as their emission already sets in before sun rise and before sufficient amounts of OH can form. Beech and spruce are mainly defined as synthesis emitters and, therefore, have more similar diurnal cycle with OH (Figures S46 and S50 in in Supporting Information S7) and show positive correlations with α-pinene and limonene. The same applies for 1,8-cineol which is nearly solely emitted by spruce (Figure S4 in Supporting Information S2) and also shows a positive correlation. The diurnal cycle for 1,8-cineol concentration of spruce is similar to the emission (Figure S50 in in Supporting Information S7). Here, the higher emissions exceed the oxidation by OH and the increase during the day is more significant than the accumulation overnight. For 10_LU limonene and α-pinene show almost the same correlation plots (Figure S13 in Supporting Information S3) as in the standard set up the difference between the two is invoked by the default monoterpene emission split and thus have similar diurnal cycles (see the 10_LU plots of Figures S45–S52 in in Supporting Information S7). Forests areas are characterized by negative (Figure S13 in Supporting Information S3) and lower emitting agricultural areas have slightly positive correlation values. 1,8-cineol and *p*-cymene show only negative values as the OH degradation exceeds emission strength. Sesquiterpenes have a positive impact on OH as their oxidation by ozone leads to OH-radical production (Karl, Tsigaridis, Vignati, & Dentener, 2009). In high NO_x environments such as the Ruhr area, this effect is limited by the fast cycling between NO_x and ozone (R1 till R6) which creates a strong positive correlation between OH and ozone. OVOCs show slightly positive correlations for coniferous forest/pine and spruce trees and negative values for mixed forest/oaks and beech. The night-time accumulation of conifers pool emissions leads to an intensified consumption of OH in the morning reducing the amount of OH for the slower reaction of OVOC which delays and impairs the onset of depletion (compare Figure S46 and Figure S47 in Supporting Information S7).

3.2.2.2. NO_3

The reaction of α-pinene with OH is rather slow and the consumption of OH radicals by isoprene and OVOCs makes the α-pinene NO_3 degradation path even more important (Ng et al., 2017). There is a direct link between α-pinene (Figures S3 and S6 in Supporting Information S2) and NO_3 concentrations (Figure S15 in Supporting Information S3). Again, showing invers colors in the difference plots. This is more pronounced for the reduced α-pinene emission of spruce trees, here the α-pinene concentration is roughly halved while at the same time NO_3 concentration doubles.

The rapid photolysis of NO_3 during the day by R11a and R11b keeps daytime NO_3 concentration low. But during night, the concentration builds up and NO_3 becomes an important BVOC oxidant. Therefore, only night-time values are considered (between 19 UTC and 3 UTC) in the correlation calculation (Figures S16 and S17 in Supporting Information S3). Night-time BVOC emissions are rather low or even not existing for synthesis emissions (isoprene, synthesis monoterpene). Additionally, the progressing BVOC degradation further reduces their concentrations during night and thus opposing trends compared to NO_3 can be observed independent of the LU for isoprene, sesquiterpenes, limonene, and α-pinene and thus are negatively correlated. Largest negative values are reached for limonene and α-pinene due to their fast NO_3 oxidation (lifetime of minutes Figure S43 in Supporting Information S7; Oderbolz et al., 2013). 1,8-Cineol, *p*-cymene and OVOCs are emitted in low quantities during night but as they nearly solely react with OH-radicals (Figures S42–S44 in Supporting Information S7; Corchnoy & Atkinson, 1990; Oderbolz et al., 2013), their concentration builds up due to lacking oxidants resulting in a positive NO_3 correlation.

However, in areas with high BVOC concentrations a negative NO_3 correlation is calculated, because of significant OH and HO_2 generation by ozonolysis processes. This also results in negative correlation between NO_3 and ozone (Stockwell et al., 1997). Furthermore, the reaction of RO_2 with NO leads to NO_2 and HO_2 production (R8). Subsequent reactions of HO_2 with NO and NO_3 are additional OH sources (Stockwell et al., 1997). Due to the enhanced BVOC emissions of the 10_LU run, a higher OH radical production occurs for coniferous forests compared to the 138_LU run increasing the area of negative correlations of NO_3 with ozone, OVOCs, 1.8-cineol,

and *p*-cymene. Night-time BVOC emissions are considerably reduced for the 138_LU as the most common tree species show higher ratios of synthesis emissions with pine being the main contributor to night-time BVOC emissions. Therefore, negative correlations are only present in pine dominated surroundings. The night-time production of OH is visible in the time series, mainly for spruce and pine, especially at the second half of May where higher temperatures and radiation amplify BVOC emissions (Figures S45–S52 in Supporting Information S7). Here, OH radicals are not completely degraded during night. The synthesis emissions of beech inhibit night-time ozonolysis thus no significant OH production occurs.

3.2.2.3. Ozone

The ozone concentration budget (Figure S18 in Supporting Information S3) strongly depends on NO_x (R4, R5, and R6) and VOC levels as well as on VOC composition (R7, R8, and R9). Differences in ozone are mainly linked to isoprene and limonene emission modification as they changed the most between the two LU data sets (Figures S2, S3 in Supporting Information S2 and Figure S18 in Supporting Information S3). The most considerable ozone reduction occurs in pine forests in east Germany (up to 2.5%). In the western domain, similar ozone values are modeled due to intensified isoprene emissions of oaks.

The 10_LU shows higher positive correlation values (Figure S19 in Supporting Information S3) than the 138_LU (Figure S20 in Supporting Information S3) with a north-east south-west gradient. The lifetime of BVOCs due to ozone is in the range of a few minutes for β-caryophyllene, hours for API and LIM, 1 day for isoprene and more than 100 days till years for 1,8-cineol, *p*-cymene, and OVOCs (Figure S44 in Supporting Information S7; Atkinson & Arey, 2003; Oderbolz et al., 2013). Therefore, a direct link to tree species is difficult as here not just the ozone consumption but also the production through other reaction pathways is tedious. Both processes overlap each other and are additionally impacted by transport processes. This makes the correlation even more sensitive to the diurnal cycle. Oaks and spruces show higher positive isoprene ozone correlation values whereas areas with lower correlation values show elevated fractions of birch, beech, and pine trees, which are all classified as non-isoprene emitters (Figure 1 and Figure S20 in Supporting Information S3). Monoterpenes, sesquiterpenes and OVOCs show negative correlations for high NO_x environments (Ruhr area, Berlin). Here, the reduction of ozone, OH- (R1, R2, and R3), and NO_3- (R10) radical concentration lowers the oxidizing ability which increases reactant concentrations. Sesquiterpenes are most sensitive to the NO_x-induced ozone depletion as they are preferably oxidized by ozone (Oderbolz et al., 2013). The plots for the 138_LU (Figure S20 in Supporting Information S3) depict more substantial regional differences in the correlations for 1,8-cineol and *p*-cymene. Both are not emitted by beech and pine, while spruce emit higher quantities generating higher positive correlation values. *p*-Cymene is also not emitted by spruces. Just a few tree species such as Douglas fir and *Pinus nigra* emit sufficient amounts of *p*-cymene mainly resulting in positive correlations. Oaks emit minute quantities of *p*-cymene which makes it an unlikely reaction partner and accumulation occurs more frequently resulting in opposing diurnal concentration cycle (Figure S52 in Supporting Information S7) and cause negative correlations in the south-west model domain. These effects associated with 1,8-cineol and *p*-cymene might change when exchanging the default emission split to measurement-based values.

Anthropogenic emissions are the same for both simulations but LU induced BVOC emission deviations affect NO_x concentrations. Lower BVOC emissions of the 138_LU especially of pine and spruce forests reduce the amount of organic peroxy radicals RO_2 (R7) and limits their NO degradation channel (R8) lowering HO_2 and NO_2 production and increase NO concentration. However, the RO_2 reduction promotes the oxidation of O_3 by NO (R5) which reduces O_3 while increasing NO_2 concentration. Therefore, HO_2 and ozone concentration is reduced whereas NO and NO_2 concentration is slightly increased for the 138_LU (Figure 3). The increase in NO_2 in combination with increased OH concentration of pine forests facilitates HNO_3 production (R13) with a maximum increase in Brandenburg (Figure 3). In the western model domain, similar NO and ozone values are observed. Here, the frequent occurrence of larger cities generates higher NO_x (Figures S21 and S22 in Supporting Information S3) but lower ozone (Figure S18 in Supporting Information S3) concentration as well as lower OH concentrations (Figure S12 in Supporting Information S3) due to oaks/mixed forests. The increase in NO_3-radical concentration for spruce trees due to their lower α-pinene emissions enables the formation of N_2O_5 (R14, Figure 3) which leads to NO_2 removal (blue colored bow around Luxembourg Figure 3). The highest NO increase (Figure 3 and Figure S21 in Supporting Information S3) can be observed for larger cities (e.g., Ruhr area and Frankfurt am Main) and landscapes shaped by surface mining (East Germany). In high NO_x environments, the increased BVOC emissions of the 10_LU amplifies NO_2 production (R8) creating the negative NO_2 differences

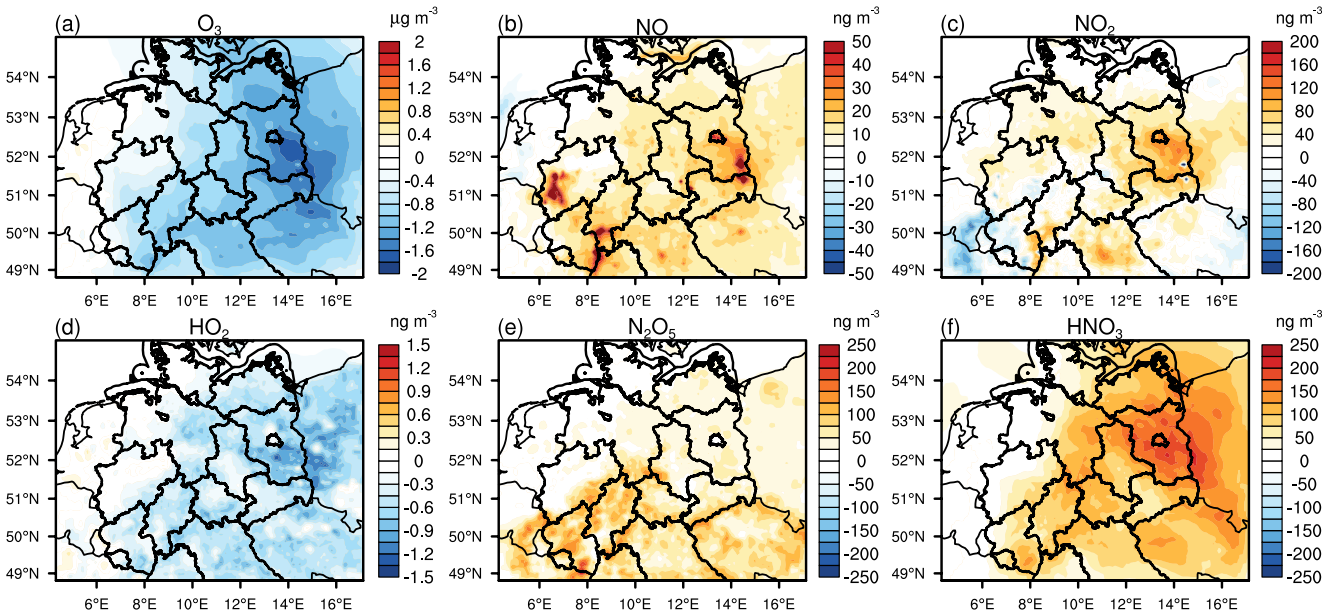

Figure 3. Difference plots between the mean values of the 138_LU and 10_LU for (a) ozone, (b) nitrogen monoxide, (c) nitrogen dioxide, (d) hydroperoxyl radical, (e) dinitrogen pentoxide, and (d) nitric acid during May 2014.

which are more pronounced in BVOC rich environments in East Germany (Figure 3 and Figure S22 in Supporting Information S3).

NO and NO_2 show negatively ozone correlations (Figures S19 and S20 in Supporting Information S3). The early morning NO emission peak quickly reduces ozone and produces NO_2 (R5). If ozone is completely depleted, NO concentration rises again but decreases when photolytic ozone production becomes efficient (R6 and R4). Due to the high day-time ozone values, NO afternoon emissions do not manifest in NO but in a NO_2 concentration rise while at the same time ozone decreases. Therefore, negative correlations are more pronounced for NO_2. Largest negative correlation values for both NO and NO_2 occur in high NO_x environments. Additional ozone production results from the reaction of RO_2 by NO molecules (R8 followed by R9, R6, and R4). Hence, lower ozone concentration combined with lower BVOC concentration indicate a production dependency rather than a consumption as for the other oxidants.

3.3. Impacts on SOA Production

Tropospheric oxidation of BVOCs leads to the formation of low volatile reaction products enabling SOA formation. The amount of SOA and its composition depends on the BVOC amount and mixture which are directly linked to the LU data sets. But the relationships between BVOCs, oxidants, and SOA concentrations are intricate, as they depend on the diurnal cycle of BVOC emission, transport, and degradation. Figure S23 in Supporting Information S4, shows the modeled total SOA concentrations. Maximum SOA concentrations are modeled for coniferous forests of the 10_LU and pine forests for the 138_LU. The monoterpenes grouped into the classes API donated α-pinene (Figure S26 in Supporting Information S4) and LIM donated limonene (Figure S27 in Supporting Information S4) contribute for almost the entire SOA difference between the two LU data sets. The fast night-time oxidation of API and LIM by NO_3 (in a few minutes Figure S43 in Supporting Information S7; Oderbolz et al., 2013) and its high SOA forming potential makes these SOA canals the most important once and is confirmed by its positive correlation (Figures S24, S25 in Supporting Information S4 and Figures S45–S52 in Supporting Information S7). α-Pinene NO_3 SOA products can be identified as the dominant SOA source for Melpitz (see Section 3.7). Maximum SOA concentrations occur during night. Thus, its diurnal cycle is opposed to OH radical concentration (negatively correlated; Figures S24 and S25 in Supporting Information S4).

Monoterpenes are emitted throughout the day for the 10_LU. API and LIM concentration correlations are mainly positive (Figure S24 in Supporting Information S4). The synthesis link of monoterpene emissions for spruce and

beech combined with the rapid NO_3 reaction results in vast or even total night-time API and LIM concentration reductions (Figures S50 and S46 in Supporting Information S7) which can induce negative correlations (Figure S25 in Supporting Information S4). 1,8-Cineol and *p*-cymene are characterized by an accumulation during night as their main oxidizing agent OH is then only scarcely produced, thus entail a positive correlation. However, direct SOA contributions are small. The higher 1,8-cineol emission of spruce and its link to diurnal syntheses cycle impairs correlation values. Otherwise BARO, BHC8, and OVOC concentrations seem to be extraordinary SOA proxies (Figures S45–S52 in Supporting Information S7). The night-time monoterpene emissions of pine trees facilitate SOA production via NO_3 oxidation turning pine into the major SOA contributor for the 138_LU. The difference between the two LU data sets is highest for spruce and beech followed by pine trees.

Isoprene (Figure S28 in Supporting Information S4) and sesquiterpenes (Figure S29 in Supporting Information S4) SOA concentrations are about one magnitude lower. Isoprene SOA concentration covers the entire land domain and is highest in the east and south-west of the domain for the 10_LU, while for the 138_LU it is only present in the south-west and far east. Brandenburg and the central model domain reveal the most significant isoprene SOA changes. Maximum sesquiterpene SOA concentrations are modeled in Brandenburg for both data sets. The huge SOA forming potential of sesquiterpenes is demonstrated by the difference plot (Figure S29 in Supporting Information S4) as even small birch fractions yield considerable increases of SOA. As monoterpene NO_3 reaction products are the dominant SOA source, its night-time production is usually opposed to isoprene and sesquiterpene peak concentrations and thus negatively correlated. In areas with smaller negative OH SOA correlation (north and west of model domain) positive values are present.

The reduced BVOC emissions of the 138_LU (342 μg m^{-2} h^{-1} compared to 430 μg m^{-2} h^{-1} for 10_LU) diminishes the available absorbing OM which not only influences biogenic (Figure S30 in Supporting Information S4) but also anthropogenic SOA (Figure S31 in Supporting Information S4). Both are reduced with a minimum in the southern domain. Here, a decrease in overall SOA concentration by up to 60% is present, primarily caused by the reduced monoterpene emission of the 138_LU and the reduced OH availability due to the increased OH depletion by OVOCs which hinders SOA formation. Average anthropogenic SOA contribution is below 15%.

Considering SOA as part of $PM_{2.5}$ and PM_{10}, changes in LU can affect PM composition. The simulated PM consists of primary emitted PM_{10} and $PM_{2.5}$, ammonium nitrate, ammonium sulfate, sulfate, sea salt, dust particles, and SOA. In general, in industrialized regions with strong anthropogenic emissions, such as the area between the Netherlands and the Ruhr area, the SOA fraction is typically less than 10%. In forests, SOA fraction values of up to 35% are reached for $PM_{2.5}$ (Figure S32 in Supporting Information S4) and 27% for PM_{10} (Figure S33 in Supporting Information S4). Total difference between the two LU are about 6% for $PM_{2.5}$ and 5% for PM_{10} with largest deviation between coniferous forests and spruce as well as pine trees.

3.4. Role of Additional Agricultural NO Soil Emissions

Changes to the oxidant concentrations by modified NO_x regimes invoke LU depending air quality changes due to the specific BVOC mixtures as well as emission strengths and their response to NO_x variations. Therefore, the whole setup is used to further investigate the interplay between LU induced changes to BVOC composition and strength combined with additional NO soil emission on air quality. The BVOC emission stays as previously stated for both LU data sets.

To test the NO model sensitivity, simulations with additional agricultural NO soil emissions have been performed for both LU data sets using the parametrizations from Williams et al. (1992) and Stohl et al. (1996). The agricultural NO soil parameterization is based on empirical relationships between soil temperature and land use type including fertilization rate of cropland. All plots already referred to in the previous sections show the additional NO emission scenario entitled with—NO on the right-hand side. The general patterns of the plots stay roughly the same. NO emission (Figure S34 in Supporting Information S5) increased (57%) especially in the NW-SE agricultural band (Figure 1 and Figure S1 in Supporting Information S1). NO emissions and concentrations as well as NO_2 concentration patterns (Figures S21 and S22 in Supporting Information S3) are comparable for both LU data sets. An increase in mean NO (40%), NO_2 (43%), and SOA (1%) and a decrease in ozone (5%) concentration was induced.

Additional NO soil emission influences the photostationary state between ozone, NO, and NO_2 (R1–R6). This leads to ozone reduction and NO_2 rise independent of the land use, which are congruent to the NO emission

increase (Figure S34 in Supporting Information S5). In already high NO_x regimes, for example, big cities followed by cropland NO concentration rises most notably (Figure S35 in Supporting Information S5). Between the two LU data sets the lower NO and NO_2 concentrations in the western model domain, the Czech Republic and northern Poland of Figures S21 and S22 in Supporting Information S3 relate to the LU category natural and agricultural vegetation (Figure 1c) for which BVOC and NO emissions are slightly lower compared to the generalized mixed LU class of 10_LU.

Areas of low BVOC emissions are characterized by OH concentration reduction (Figure S35 in Supporting Information S5). This applies for cropland, mud flats, pastures, wetlands, cities, and motorways. Here, the oxidation of O_3 by NO reduces the ozone concentration (R5) which hinders ozone photolysis (R1a) and OH production (R3). Furthermore, the lower BVOC concentrations cannot compensate the OH radical loss via OH production (R8 and R9). The production of NO_3 is linked to the reaction of NO_2 with ozone (R10) or the reaction of HNO_3 with OH (Stockwell et al., 1997). Here the reduction in ozone and OH concentration results in NO_3 loss (Figure S35 in Supporting Information S5) reducing the overall oxidant concentration in low BVOC concentration areas.

In areas of intensified BVOC emissions additional NO molecules facilitate the reaction between RO_2 and NO (R8) which enhances not only the NO_2 and HO_2 (Figures S34 and S35 in Supporting Information S5) but also the ozone production (R1 till R9). HO_2 declines with rising BVOC and declining NO_x concentrations generally in the east and center of the model domain (Figure S35 in Supporting Information S5). The formed OH radicals (R9) can initiate additional BVOC oxidation generating a self-reinforcing effect. Even though ozone concentration declines with increased NO emission for both LU data sets, the difference between the two widens (Figure S18 in Supporting Information S3). Here, the higher isoprene and limonene emission of conifer forests in Brandenburg for the 10_LU and the isoprene oak emission spots in the west for the 138_LU trigger ozone production. The boosted OH concentration in BVOC rich environments through R7, R8, and R9 also enhances HNO_3 production (R13) with largest increase in the eastern model domain (Figure S35 in Supporting Information S5). Here, the higher OH, HNO_3, and ozone concentrations result in boosted NO_3 concentrations (Figure S35 in Supporting Information S5) increasing the overall oxidant concentration in high BVOC concentration areas.

This increase in oxidants in BVOC-rich and low-NO_x environments enhances BVOC degradation which lowers their concentration in coniferous forests for the 10_LU and for pine and oak for the 138_LU (Figure S36 in Supporting Information S5). The larger BVOC emissions of the 10_LU creates a higher NO initiated boost. Under higher NO_x conditions, the reduction of OH, NO_3, and ozone hinders BVOC oxidation and leaves them untouched which increases BVOC concentrations mainly in the west and the NW-SE cropland band (Figure S36 in Supporting Information S5).

As a result, isoprene and monoterpene SOA concentration rise in areas of lower NO_x and high BVOC concentrations and diminish in the west with a minimum in the south of the Netherlands (Figures S26–S28 in Supporting Information S4). Even though, Sesquiterpene oxidation is affected by the ozone reduction in BVOC-rich and high-NO_x areas, a sesquiterpene-SOA increase is achieved in Brandenburg and Poland (Figure S29 in Supporting Information S4). Here, the isoprene and monoterpene SOA growth increased the available OM intensifying SOA formation. The overall SOA concentration increases in BVOC rich environments and decreases for lower BVOC concentrations particularly close to the NO sources with a minimum in the south of the Netherlands (Figure S36 in Supporting Information S5).

3.5. Impact of Agricultural Biomass Density Enhancements

Next to NO soil emission agriculture can impact BVOC emission strength by changes to the BD of the corresponding LU classes, for which different values are given in the literature (Karl, Guenther et al., 2009; Oderbolz et al., 2013; Steinbrecher et al., 2009). Therefore, a second sensitivity study was carried out investigating the influence of agricultural biomass enhancement. The BD of agro-forestry areas, pastures, non-irrigated land, permanently irrigated land, and agriculture mixed with natural vegetation was increased from 100, 40, 400, 400, and 50 g m^{-3} to 500, 250, 500, 500, and 375 g m^{-3}, respectively (main agricultural LU classes in the model domain N2 are: pastures, non-irrigated land, and agriculture mixed with natural vegetation). As an orientation values from Oderbolz et al. (2013) for agriculture (500 g m^{-3}) and grassland (250 g m^{-3}) are used. All LU classes have the same BVOC SEPs, therefore the increase in BVOC emissions is in line with the BD rise. Largest intensification can be found for pastures and mixed agricultural natural vegetation followed by non-irrigated

cropland (Figure 1 and Figure S37 in Supporting Information S5). OVOC emission increased the most followed by α-pinene, limonene, and isoprene. No changes occur for sesquiterpenes, as agriculture was defined as non-sesquiterpene emitting (see Section 2.3). The additional BVOCs reduce OH (3.5%) and NO_3 (10%) concentrations while ozone increases by 0.5% (Figure S37 in Supporting Information S5). For ozone, the production mechanism (R7 followed by R8, R9, and R4) compensates the consumption by BVOCs. This BVOC-triggered ozone increase reduces NO_x concentrations especially in already highly NO_x loaded environments (R5 till R10) and boosts BVOC oxidation resulting in enhanced SOA concentrations of up to 8% (Figure S37 in Supporting Information S5).

Not only tree species but also different crop species are likely to impact air quality. So far, the model domain contains information about non-irrigated arable land and complex cultivated pattern but no crop speciation which can impact BD and subsequent BVOC emission composition and strength. Therefore, more research is needed to further investigate crop induced air quality changes.

3.6. Impact of Spatial and Temporal Model Resolution

For better comparability with measurements and clearer identification of regional effects, a simulation with finer resolution was performed for a smaller model domain (N3) covering eastern Germany including the TROPOS filed site Melpitz (Figure S1 in Supporting Information S1). A nested grid starting from a resolution of 2.8 km, 1.4 km, and reaching 700 m for an area around Leipzig was used. Temporal resolution will adapt accordingly to the implemented IMEX scheme (see Section 2.1). The resolution can impact the meteorological parameters which itself control BVOC emissions and dispersion. The setup with the enhanced BDs for agricultural LU classes is used. The results of the simulation with finer resolution are shown in Figure S38 in Supporting Information S5.

Isoprene emission spots occur in the riparian forests SW and NW of Melpitz which are again linked to lower OH concentrations. α-Pinene emission is most intense for Brandenburg's pine forests reducing NO_3 concentrations. One limonene, 1,8-cineol, and *p*-cymene emission spot is present NW of Melpitz which can be matched to *Pinus nigra*. Birch trees NW and south of Melpitz lead to enhanced sesquiterpene emissions followed by pine and spruce trees. OVOC emission is highest in the southern domain for spruce trees. The resolution now also allows to draw conclusions on the influence of high NO_x emitting roads (motorways, main roads) and demonstrates the importance of higher resolution simulations for regional air quality assessments. Motorways can clearly be identified in the OH concentration plot by the darker red and the lighter blue colors of the HO_2 and NO_3 plot. In mixed regimes, where motorways are located close to areas with higher BVOC emission (mainly Brandenburg) ozone and OH radicals are produced (R4 till R9). But directly along motorways, a reduction of ozone and NO_3 radical concentrations (R4–R6 and R10) occurs. Highest ozone concentrations are reached in south Brandenburg and in the south-east corner of the model domain where motorways are close but do not encounter. A possible link to ozone might also be valid for limonene emissions, but due to lacking sources no conclusion can be drawn. As isoprene emissions mainly collides with NO_x emission sources, the effect of isoprene induced ozone production overlaps with ozone depletion by NO_x. SOA concentration is highest for Brandenburg's pine trees.

Finer resolution enables a closer look at feedback mechanisms between NO_x, BVOC, and LU. High NO_x sources mainly motorways are clearly visible now and the detailed LU allows conclusions regarding curtain LU classes and their air quality impacts. There is evidence, that the small *Pinus nigra* forest close to the motorway with its high limonene emissions and which degradation is boosted by the increased OH concentration at motorways facilitates ozone and SOA production. These local effects are not visible in the coarser resolution of the N2 simulations. Higher resolution is therefore crucial when looking at feedback mechanisms between biosphere and troposphere and consequently for regional air quality assessments. All simulations including the high-resolution run are used for comparisons with field measurements (see below).

3.7. Comparisons With Measurements From Melpitz

The output of the different model scenarios were compared to measured NO, NO_2 (Thermo-Scientific 42i-TL analyzer equipped with a blue-light convertor), and O_3 (Horiba APOA-350E) concentrations for the whole simulation period 01.05.2015 00:00 UTC until 31.05.2014 00:00 UTC (721 DP for ozone and 717 DP for NO and NO_2).Additionally the near PM_1 organic mass concentration measured by an Aerodyne High-Resolution Time of Flight Aerosol Mass Spectrometer (HR-ToF-AMS, DeCarlo et al., 2006) during the time period 07.05.2014 15:00 UTC until 27.05.2014 09:00 UTC (474 data points DP) was used for SOA concentration evaluation.

Meteorological parameters temperature, relative humidity, wind speed, and wind direction are measured at 6 m, global radiation at 2 m, and precipitation at 1 m height. The simulation output is at 10 m height. The simulated wind speed was corrected using a roughness length of 0.03 m, the most likely value for natural grassland and pastures (Silva et al., 2007). Tables S5 and S6 in Supporting Information S1 show statistical analysis (min., mean., max, standard deviation, correlation R, and slope) for the time period May 2014 and Figure 4 and Figures S39, S40, S41 in Supporting Information S6 show the time series for OM concentration, meteorological parameters, gas-phase concentrations and SOA composition, respectively. Figure S45 in Supporting Information S7 shows the normalized time series and correlation matrixes for both LU data sets. Correlations between the measurements and the different simulations improve with resolution. Modeled wind speed is slightly higher (mean of 4.6 m $s^{-1}$for N1, 4.5 m s^{-1} for N2, and 4.2 ms^{-1} for N3) with an approximate offset of about 1 m s^{-1} and a stronger north-west wind component (Figure S39 in Supporting Information S6) compared to the measurements (mean 2.9 m s^{-1}). Temperature variation is similar for all simulations ($R > 0.9$). N1 shows an over as well as underestimation of temperatures on certain days (Figure S39 in Supporting Information S6) while N2 and N3 capture the diurnal cycle well, but due to overestimated night temperatures (up to 3°C) higher mean temperature values are reached.

Gas-phase concentration of NO, NO_2, and ozone (Figure S40 in Supporting Information S6) as well as OM (Figure 4) correlate best for higher BVOC and additional NO emission of the N2_10_NO simulation (Table S5 in Supporting Information S1). But due to the additional NO emissions, the mean values of NO and NO_2 for N2_10_NO and N2_138_NO are highly overestimated, as they more than double. This consequently reduces ozone mean concentration by 6 µg m^{-3} (8%). During the entire time period, maximum differences of up to 31 µg m^{-3} (39%) occur. The gas-phase concentrations are clearly affected by NO emission but the two different LU data sets have only a minor impact for Melpitz as the dominant LU is agriculture, which is alike for both data sets.

The extension of the original SORGAM mechanism significantly improves OM concentration simulations and enhance the average value from 3.1 to 5.8 µg m^{-3} for the 10_LU_NO. During the first half of May 2014 the simulations are similar and reveal a strong anthropogenic SOA contribution (Figure 4 and Figure S41 in Supporting Information S6) of up to 70% for the original SORGAM and 50% for the extended SORGAM mechanism. Clear differences between the two SOA modules are evident for the second half of the month. The original mechanism shows moderated diurnal cycles, while for the extension clear peaks (20.-23.05, 26.-27.05.2014) are visible, which are in better agreement with the measurements. OM peak concentrations occur during night. N3 simulation captures the peaks best especially at the 26.05.2014. The anthropogenic portion of OM shrinks, reaching between 10% and 55% for the original and 5%–35% for the extended SORGAM mechanism. The main biogenic SOA sources of the original SORGAM are α-pinene + ozone, followed by limonene + ozone, α-pinene + OH, and limonene + OH reaction products. Other biogenic SOA sources are not included. The extended version reveals α-pinene + NO_3 SOA products as the dominating SOA source at the field site Melpitz reaching values between 10% and 65% of the total organic mass with a maximum during night. A closer look at the meteorological conditions (Figure S39 in Supporting Information S6) during OM peak events reveal low wind speeds (below 0.5 m s^{-1}), high temperatures and intense solar radiation during the day. This triggers BVOC emissions and reduces their spatial distribution. Therefore, they stay more local and due to progressing chemical degradation reaction products accumulate (SOA, O_3, and NO_2). Correlation between AMS measurements and the simulation improves from $R = 0.3$ for the original to about 0.7 for simulations with the extended SORGAM version. Note that AMS measures OM concentration of PM_1 while the simulations predict OM of PM_{10}, therefore higher simulated values are anticipated.

4. Summary and Conclusions

To examine the interaction between biosphere and atmosphere, first a tree species-specific BVOC emission split was implemented into the model system COSMO-MUSCAT and integrated into the chemistry mechanism RACM-MIM2ext and secondly applied in detailed gas-phase model simulations. Furthermore, the SOA module SORGAM was further extended. It now includes more BVOC reaction products and SOA precursors, and even provides detailed information about both the BVOC precursors and the oxidizing agents. In this way, the importance of the individual components, oxidants, and reaction pathways can be analyzed. For the simulations, a detailed LU data set containing more than 100 tree species was compared with a LU data set including only common LU categories, such as conifer and mixed forests. Additional agricultural sensitivity studies were carried

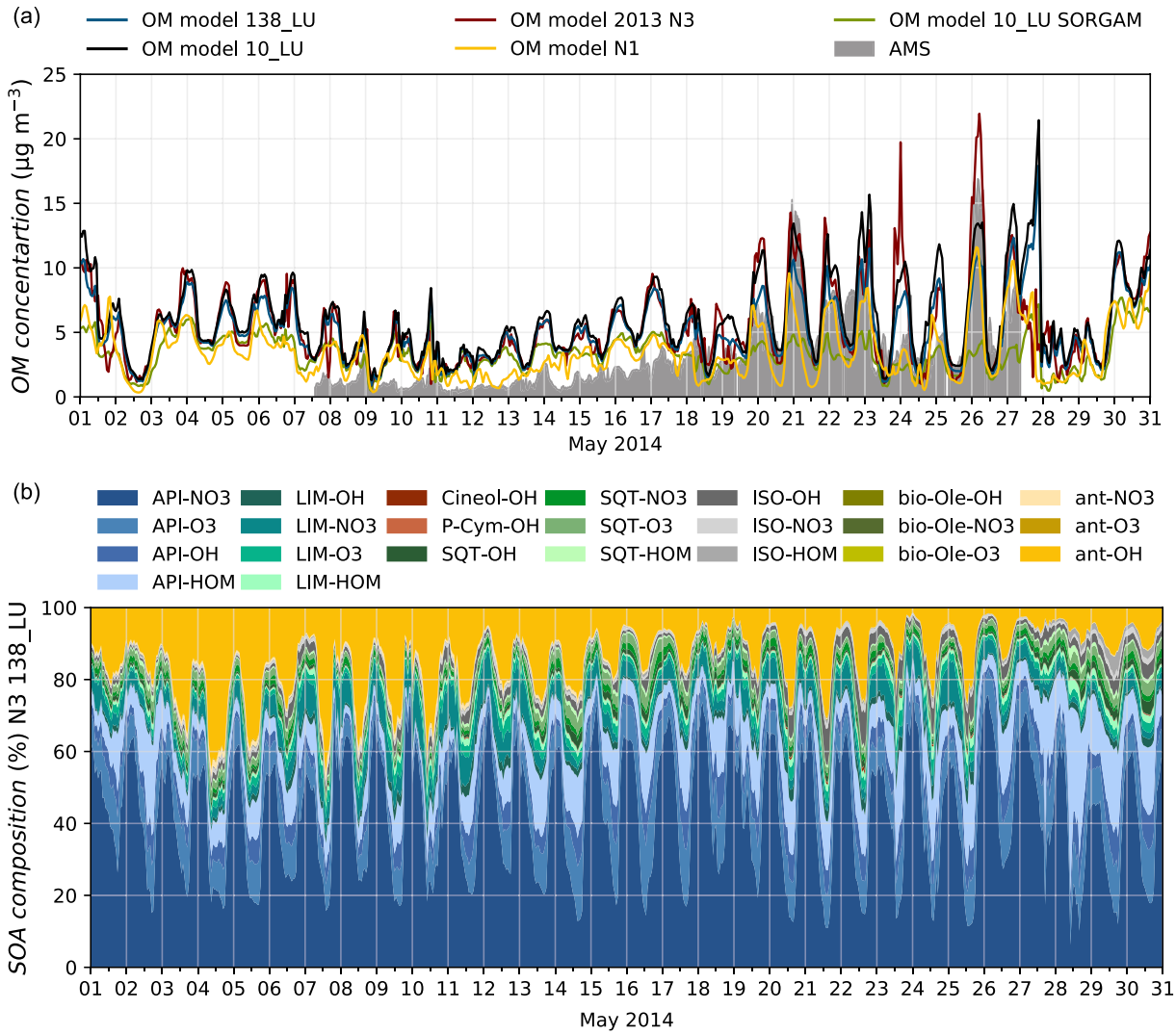

Figure 4. Time series for (a) measured and simulated organic matter concentration and (b) SOA composition of the N3 simulation for Melpitz during the time period May 2014.

out to investigate both the impact of NO soil emission and BD change on the interplay between NO_x and BVOC emission as well as ozone, OH, NO_3, and SOA concentration, respectively.

The results from the comparison of the two different LU data sets demonstrates impressively that the detail of the implemented LU data set considerably affects BVOC emission strengths, composition, as well as emission patterns. Their degradation processes impact the chemical composition of the troposphere including air pollution, such as NO_x, ground level ozone and PM (in terms of SOA). Here, the generalized LU implementation 10_LU in the case of Germany leads to 50% overestimated BVOC (excluding OVOCs) emissions generating altered oxidant concentrations (NO_x ±2.5%, ozone +2.5%, OH ±50%, and NO_3 radical −70%) and a 60% overestimation in SOA concentration compared to detailed tree species information. Jiang et al. (2019) also found only minor impacts on ozone but significant changes in SOA concentrations when comparing two different biogenic emission models for Europe.

BVOC emission spots are evident where tree species emit higher amounts of BVOCs than their corresponding forest category: (a) oaks for isoprene, (b) birch and spruce for sesquiterpenes, (c) beech and spruce for OVOCs, (d) beech for API (mainly sabinene), and (e) spruce for 1,8-cineol. Every single BVOC has its preferred oxidizing partner. Therefore, BVOC degradation strongly effects the distribution and concentration of their oxidants, such as ozone, OH, and NO_3 radicals. The present study revealed that isoprene concentration is inversely correlated

to OH and monoterpene to NO_3 radical concentrations. The lack of isoprene emission of pine trees induces an increase in OH while oaks have the utmost isoprene emission strength decreasing OH radical concentration and generating ozone during chemical conversion. The second major OH sinks are OVOCs and its degradation hinders SOA production diminishing SOA concentration in spruce forests compared to their generalized LU class coniferous forest. Even though OVOCs do not contribute to SOA formation, they are an excellent proxy for temporal SOA evolvement. Monoterpenes are emitted in huge amounts by conifers and in the case of α-pinene also by beech. Monoterpene NO_3 reaction products are the major SOA components in the model domain. Therefore, coniferous forests of the 10_LU and pine of the 138_LU are the major SOA sources but a 30% reduction of SOA manifests for pine forests mainly due to lacking limonene SOA products. LU controls the parameters defining the BVOC emission strengths and composition thereby regulating oxidant concentrations while their chemical degradation path defines their ozone and SOA forming potential. BVOCs are a crucial link to air quality and climate as this will not only impact radiation but also cloud and precipitation formation.

Sensitivity studies regarding agricultural BD enhancement reveals a regional increase in BVOC emissions (50%), ozone (0.5%), and SOA (8%) while OH (3.5%) and NO_3 (10%) concentrations decline. Additional agricultural NO soil emissions (57%) induce an equivalent NO_2 concentration (42%) increase but on the other hand an ozone (5%) and NO_3 (20%) radical concentration reduction. High NO_x environments show most significant NO increases and in combination with low BVOC concentrations OH radical concentration declines. Here the overall reduction of oxidizing agents inhibits BVOC degradation and consequently lowers SOA concentrations. In BVOC dominated lower NO_x areas, the BVOC degradation under increased NO emissions leads to the production of OH radicals and ozone. However, the production of ozone coincides with ozone depletion by NO. The additional ozone and OH radicals enhance BVOC oxidation which facilitates SOA production (+1%). The higher BVOC emission strength of the 10_LU leads to intensified ozone and SOA production compared to the 138_LU which further enhances the differences between the two data sets while at the same time OH and NO_3 concentration differences decrease in BVOC dominated areas. Here, we focused on tree species-specific impacts on air quality but also crop induced air quality changes have to be considered for air quality assessments. But, more knowledge is needed on crop specific parameters and parameterizations.

Comparisons with measurements from Melpitz reveal a significant improvement of simulated organic matter concentrations (from R of 0.3 to 0.7) when extending the SOA module. Monoterpene products are identified as the main SOA components (up to 90%), solely α-pinene + NO_3 SOA products make up to 65%. Low wind velocities, warm temperatures and high solar radiation can facilitate BVOC-induced air quality impairment which makes these cases even more sensitive to the underlying LU. Slightly changed wind conditions can alter the dispersion of VOCs as well as their oxidizing agents, and temperature can influence not only the emission of BVOCs but also their reaction speed and their partitioning into the particle phase. An overestimation of the wind speed and night time temperature leads partly to an underestimation of SOA concentration. The exact capture of meteorological conditions is therefore, another key point. Meteorological performance benefits from higher spatial and temporal resolution. Here, an improvement was achieved with every refinement from N1 to N2 and finally N3. High resolution simulations are crucial for analyzing local effects on the BVOC degradation in clean as well as in NO_x-influenced environments and enables a more detailed investigation into feedback mechanisms between NO_x, BVOC, and LU.

Overall, the simulations showed that BVOCs play a major role in air quality assessment which should be addressed by a diverse SEP, BD, and a tree species-specific emission split. Unfortunately, BVOC emission strengths as well as their exact composition remain uncertain. BVOC emissions are strongly impacted by the emission parameterization, the driving meteorological parameters and LU. For air quality assessments, also the applied chemistry mechanism and SOA module are of key importance. To further address this complex issue and to include more species-specific dependencies linked to BVOC emission parametrization as well as meteorological effects more research is needed. Here, we followed the recommendations from Steinbrecher et al. (2009) and managed to obtain a flexible model setup which allows targeted tree species-specific BVOC emissions directly integrated and online coupled to guarantee immediate biosphere-atmosphere interactions. While we incorporated the BVOC emission scheme, we identified further potential species-specific integration possibilities for several aspects regarding LU, BVOC emission parameterization, meteorology, chemistry, and SOA treatment which, to our knowledge, have not been taken into account so far and are discussed in more detail in the Supporting Information S8 (see Text S1).

5. Outlook

This work demonstrates the high sensitivity of BVOC emissions toward LU cover implying huge potential for further LU database improvements when considering tree species-specific data. Furthermore, an advanced knowledge about the individual species-specific response to a variety of stressors, such as ozone, drought, wounding, CO_2, etc. is important to further improve BVOC emission estimates as this will modify BVOC emission strengths and composition and thus affect air quality through ozone and SOA formation. This impacts not only radiation but also cloud and precipitation formation processes and thus entails a feedback mechanism back to climate. Therefore, more knowledge is needed about the biosphere-atmosphere interaction in view of a changing climate. But so far, only a few studies on stress response exist. The findings of the present air quality study, aimed to study the impacts of a forest versus detailed tree species LU data set, are linked not only to LU data sets but to the chemical mechanism and SOA treatment as well. To further improve the chemical degradation of biogenic and anthropogenic VOCs, the currently applied gas-phase chemistry mechanism RACM-MIM2-ext will soon be replaced by a more advanced chemical mechanism which is based on the MOZART mechanism (Schultz et al., 2018). This further improvement will help to overcome the discrepancies between the measured and simulated gas-phase concentrations. Simultaneously, the SOA module has to be adjusted and extended in accordance with the new gas-phase mechanism. These developments shall further improve air quality assessments on a regional to global scale. The feedback between transport processes, biosphere and atmosphere will be further investigated focusing on the interaction of biogenic and anthropogenic emissions and their influence on air quality (PM, O_3, and NO_x). For better comparisons with measurements, a size-resolved SOA model treatment would considerably benefit further analyses.

Conflict of Interest

The authors declare no conflicts of interest relevant to this study.

Data Availability Statement

Modeling data supporting the findings of this article are available online and should be cited as Luttkus, M. L. (2021) COSMO-MUSCAT model data for different scenarios [Data set]. Zenodo. https://doi.org/10.5281/zenodo.4783106. All data can be made available upon a reasonable request. Measurement data for Melpitz can also be extracted from http://ebas.nilu.no/ (instrument type chemiluminescence_molybdenum Data set-ID: 220148588 till 220148591 for pressure, temperature, relative humidity, and NO and 220148595 for NO_2). Supporting information is available with the online version of this article. Note there are eight supporting information files, the first one Supporting Information S1 contains a figure of the model domain (Figure S1) and the tables S1–S4 for the SOA module as well as statistical information about the model simulations. The plots for the BVOC emissions (Figure S2–S4) and concentrations (Figures S5–S11) are included in Supporting Information S2, the concentration and correlation plots of the oxidizing agents (Figures S12–S22) are part of Supporting Information S3 and for SOA (Figures S23–S33) of Supporting Information S4. Supporting Information S5 contains plots for agricultural NO emission and biomass density sensitivity studies (Figures S34–S37), as well as for the model domain N3 (Figure S38). All plots (Figures S39–S41) and tables (Tables S5 and S6) for the field side Melpitz can be obtained from Supporting Information S6. The plots for selected spots marked in Figure S1 in Supporting Information S1 are included in Supporting Information S7 together with a discussion about the current restrictions of species-specific model representation in Supporting Information S8.

Acknowledgments
This project is funded by the Ph.D. scholarship program (AZ 20016/452) of the German Federal Environment Foundation (Deutsche Bundesstiftung Umwelt, DBU). The work was supported by the Center for Information Services and High Performance Computing (ZIH). Open access funding enabled and organized by Projekt DEAL.

References

Atkinson, R. (2000). Atmospheric chemistry of VOCs and NO_x. *Atmospheric Environment*, *34*(12), 2063–2101. https://doi.org/10.1016/S1352-2310(99)00460-4

Atkinson, R., & Arey, J. (2003). Gas-phase tropospheric chemistry of biogenic volatile organic compounds: A review. *Atmospheric Environment*, *37*(Suppl. 2), S197, 219. https://doi.org/10.1016/S1352-2310(03)00391-1

Bastin, J.-F., Routh, D., Zohner, C. M., & Crowther, T. W. (2019). The global tree restoration potential. *Science*, *365*, 76–79. https://doi.org/10.1126/science.aax0848

Berndt, T., Herrmann, H., Sipilä, M., & Kulmala, M. (2016). Highly oxidized second-generation products from the gas-phase reaction of OH radicals with isoprene. *The Journal of Physical Chemistry A*, *120*, 10150–10159. https://doi.org/10.1021/acs.jpca.6b10987

Berndt, T., Richters, S., Jokinen, T., Hyttinen, N., Kurtén, T., Otkjær, R. V., et al. (2016). Hydroxyl radical-induced formation of highly oxidized organic compounds. *Nature Communications*, *7*(13677), 1–8. https://doi.org/10.1038/ncomms13677

Birmili, W., Schepanski, K., Ansmann, A., Spindler, G., Tegen, I., Wehner, B., et al. (2008). A case of extreme particulate matter concentrations over Central Europe caused by dust emitted over the southern Ukraine. *Atmospheric Chemistry and Physics*, *8*, 997–1016. https://doi.org/10.5194/acp-8-997-2008

Corchnoy, S. B., & Atkinson, R. (1990). Kinetics of the gas-phase reactions of OH and NO_3 radicals with 2-carene, 1,8-cineol, p-cymene, and terpinolene. *Environmental Science & Technology*, *24*, 1497–1502. https://doi.org/10.1021/es00080a007

DeCarlo, P. F., Kimmel, J. R., Trimborn, A., Northway, M. J., Jayne, J. T., Aiken, A. C., et al. (2006). Field-deployable, high-resolution, time-of-flight aerosol mass spectrometer. *Analytical Chemistry*, *78*, 8281–8289. https://doi.org/10.1021/ac061249n

De Meij, A., Bossioli, E., Penard, C., Vinuesa, J. F., & Price, I. (2015). The effect of SRTM and CORINE Land Cover data on calculated gas and PM10 concentrations in WRF-Chem. *Atmospheric Environment*, *101*, 177–193. https://doi.org/10.1016/j.atmosenv.2014.11.033

De Meij, A., & Vinuesa, J. F. (2014). Impact of SRTM and CORINE Land Cover data on meteorological parameters using WRF. *Atmospheric Research*, *143*, 351–370. https://doi.org/10.1016/j.atmosres.2014.03.004

Doms, G., Förstner, J., Heise, E., Herzog, H. J., Mironov, D., Raschendorfer, M. (2018). *A description of the nonhydrostatic regional COSMO-model Part II physical parameterizations COSMO 5.05*. Deutscher Wetterdienst. Retrieved from https://www.cosmo-model.org/content/model/documentation/core/cosmo_physics_5.05.pdf

Doms, G., Förstner, J., Heise, E., Herzog, H. J., Mironov, D., Raschendorfer, M., et al. (2013). *A description of the nonhydrostatic regional COSMO-model Part II physical parameterizations COSMO 5.05*. Deutscher Wetterdienst. https://doi.org/10.5676/DWD_pub/nwv/cosmo-doc_5.05_II

Ehn, M., Thornton, J. A., Kleist, E., Sipilä, M., Junninen, H., Pullinen, I., et al. (2014). A large source of low-volatility secondary organic aerosol. *Nature*, *506*, 476–479. https://doi.org/10.1038/nature13032

Faiola, C. L., Jobson, B. T., & Van Reken, T. M. (2015). Impacts of simulated herbivory on volatile organic compound emission profiles from coniferous plants. *Biogeosciences*, *12*(2), 527–547. https://doi.org/10.5194/bg-12-527-2015

Findell, K. L., Berg, A., Gentine, P., Krasting, J. P., Lintner, B. R., Malyshev, S., et al. (2017). The impact of anthropogenic land use and land cover change on regional climate extremes. *Nature Communications*, *8*, 989. https://doi.org/10.1038/s41467-017-01038-w

Fitzky, A. C., Sandén, H., Karl, T., Fares, S., Calfapietra, C., Grote, R., et al. (2019). The interplay between ozone and urban vegetation-BVOC emissions, ozone deposition, and tree ecophysiology. *Frontiers in Forests and Global Change*, *2*, 50. https://doi.org/10.3389/ffgc.2019.00050

García-García, A., Cuesta-Valero, F. J., Beltrami, H., González-Rouco, F., García-Bustamante, E., & Finnis, J. (2020). Land surface model influence on the simulated climatologies of temperature and precipitation extremes in the WRF v3.9 model over North America. *Geoscientific Model Development*, *13*(11), 5345–5366. https://doi.org/10.5194/gmd-13-5345-2020

Geron, C., Rasmussen, R., Arnts, R. R., & Guenther, A. (2000). A review and synthesis of monoterpene speciation from forests in the United States. *Atmospheric Environment*, *34*(11), 1761–1781. https://doi.org/10.1016/S1352-2310(99)00364-7

Griffin, R. J., Cocker, D. R., III, Flagan, R. C., & Seinfeld, J. H. (1999). Organic aerosol formation from the oxidation of biogenic hydrocarbons. *Journal of Geophysical Research: Atmospheres*, *104*(D3), 3555–3567. https://doi.org/10.1029/1998JD100049

Guenther, A. B. (1997). Seasonal and spatial variations in natural volatile organic compound emissions. *Ecological Applications*, *7*(1), 34–45. https://doi.org/10.1890/1051-0761(1997)007[0034:SASVIN]2.0.CO;2

Guenther, A. B., Jiang, X., Heald, C. L., Sakulyanontvittaya, T., Duhl, T., Emmons, L. K., & Wang, X. (2012). The model of emissions of gases and aerosols from nature version 2.1 (MEGAN2.1): An extended and updated framework for modeling biogenic emissions. *Geoscientific Model Development*, *5*(6), 1471–1492. https://doi.org/10.5194/gmd-5-1471-2012

Guenther, A. B., Zimmerman, P. R., Harley, P. C., Monson, R. K., & Fall, R. (1993). Isoprene and monoterpene emission rate variability: Model evaluations and sensitivity analyses. *Journal of Geophysical Research*, *98*(D7), 12609–12617. https://doi.org/10.1029/93JD00527

Harley, P., Eller, A., Guenther, A., & Monson, R. K. (2014). Observations and models of emissions of volatile terpenoid compounds from needles of ponderosa pine trees growing in situ: Control by light, temperature and stomatal conductance. *Oecologia*, *176*(1), 35–55. https://doi.org/10.1007/s00442-014-3008-5

Held, A., Nowak, A., Brimili, W., Wiedensohler, A., Forkel, R., & Klemm, O. (2004). Observations of particle formation and growth in a mountainous forest region in central Europe. *Journal of Geophysical Research*, *109*, D23204. https://doi.org/10.1029/2004JD005346

Hoffmann, T., Odum, J. R., Bowman, F., Collins, D., Klockow, D., Flagan, R. C., & Seinfeld, J. H. (1997). Formation of organic aerosols from the oxidation of biogenic hydrocarbons. *Journal of Atmospheric Chemistry*, *26*(2), 189–222. https://doi.org/10.1023/A:1005734301837

Im, U., Bianconi, R., Solazzo, E., Kioutsioukis, I., Badia, A., Balzarini, A., et al. (2014a). Evaluation of operational online-coupled regional air quality models over Europe and North America in the context of AQMEII phase 2. Part I: Ozone. *Atmospheric Environment*, *115*, 404–420. https://doi.org/10.1016/j.atmosenv.2014.09.042

Im, U., Bianconi, R., Solazzo, E., Kioutsioukis, I., Badia, A., Balzarini, A., et al. (2014b). Evaluation of operational online-coupled regional air quality models over Europe and North America in the context of AQMEII phase 2. Part II: Particulate matter. *Atmospheric Environment*, *115*, 420–441. https://doi.org/10.1016/j.atmosenv.2014.08.072

Jiang, J., Aksoyoglu, S., Ciarelli, G., Oikonomakis, E., El-Haddad, I., Canonaco, F., et al. (2019). Effects of two different biogenic emission models on modelled ozone and aerosol concentrations in Europe. *Atmospheric Chemistry and Physics*, *19*(6), 3747–3768. https://doi.org/10.5194/acp-19-3747-2019

Jokinen, T., Berndt, T., Makkonen, R., Kerminen, V.-M., Junninen, H., & Paasonen, P. (2015). Production of extremely low volatile organic compounds from biogenic emissions: Measured yields and atmospheric implications. *Proceedings of the National Academy of Sciences of the United States of America*, *112*(23), 7123–7128. https://doi.org/10.1073/pnas.1423977112

Karl, M., Dorn, H.-P., Holland, F., Koppmann, R., Poppe, D., Rupp, L., et al. (2006). Product study of the reaction of OH radicals with isoprene in the atmosphere simulation chamber SAPHIR. *Journal of Atmospheric Chemistry*, *55*, 167–187. https://doi.org/10.1007/s10874-006-9034-x

Karl, M., Guenther, A., Koble, R., Leip, A., & Seufert, G. (2009). A new European plant-specific emission inventory of biogenic volatile organic compounds for use in atmospheric transport models. *Biogeosciences*, *6*, 1059–1087. https://doi.org/10.5194/bg-6-1059-2009

Karl, M., Tsigaridis, K., Vignati, E., & Dentener, F. (2009). Formation of secondary organic aerosol from isoprene oxidation over Europe. *Atmospheric Chemistry and Physics*, *9*(18), 7003–7030. https://doi.org/10.5194/acp-9-7003-2009

Knoth, O., & Wolke, R. (1998a). An explicit-implicit numerical approach for atmospheric chemistry-transport modelling. *Atmospheric Environment*, *32*(10), 1785–1797. https://doi.org/10.1016/S1352-2310(97)00476-7

Knoth, O., & Wolke, R. (1998b). Implicit-explicit Runge-Kutta methods for computing atmospheric reactive flows. *Applied Numerical Mathematics*, *28*(2–4), 327–341. https://doi.org/10.1016/S0168-9274(98)00051-8

Köble, R., & Seufert, G. (2001). *Novel maps for forest tree species in Europe*. Paper presented at Proceedings of the 8th European Symposium on the Physico-Chemical Behaviour of Air Pollutants: "A changing atmosphere!", Torino, Italy.

Kroll, J. H., Ng, N, L., Murphy, S. M., Flagan, R. C., & Seinfeld, J. H. (2006). Secondary organic aerosol formation from isoprene photooxidation. *Environmental Science & Technology*, *40*(6), 1869–1877. https://doi.org/10.1021/es0524301

Kuenen, J. J. P., Visschedijk, A. J. H., Jozwicka, M., & Denier van der Gon, H. A. C. (2014). TNO-MACC-II emission inventory; A multi-year (2003–2009) consistent high-resolution European emission inventory for air quality modelling. *Atmospheric Chemistry and Physics*, *14*, 10963–10976. https://doi.org/10.5194/acp-14-10963-2014

Lehtipalo, K., Yan, C., Dada, L., Bianchi, F., Xiao, M., & Wagner, R. (2018). Multicomponent new particle formation from sulfuric acid, ammonia, and biogenic vapors. *Science Advances*, *4* (12), eaau5363. https://doi.org/10.1126/sciadv.aau5363

Li, D., Bou-Zeid, E., Barlage, M., Chen, F., & Smith, J. A. (2013). Development and evaluation of a mosaic approach in the WRF-Noah framework. *Journal of Geophysical Research: Atmospheres*, *118*(21), 11918–11935. https://doi.org/10.1002/2013JD020657

Macchioni, F., Cioni, P. L., Flamini, G., Morelli, I., Maccioni, S., & Ansaldi, M. (2003). Chemical composition of essential oils from needles, branches and cones of *Pinus pinea, P. halepensis, P. pinaster* and *P. nigra* from central Italy. *Flavor and Fragance Journal*, *18*(2), 139–143. https://doi.org/10.1002/ffj.1178

Miralles, D. G., Gentine, P., Seneviratne, S. I., & Teuling, A. J. (2019). Land-atmospheric feedbacks during droughts and heatwaves: State of the science and current challenges. *Annals of the New York Academy of Sciences*, *1436*(1), 19–35. https://doi.org/10.1111/nyas.13912

Ng, N. L., Brown, S. S., Archibald, A. T., Atlas, E., Cohen, R. C., Crowley, J. N., et al. (2017). Nitrate radicals and biogenic volatile organic compounds: Oxidation, mechanisms, and organic aerosol. *Atmospheric Chemistry and Physics*, *17*, 2103–2162. https://doi.org/10.5194/acp-17-2103-2017

Ng, N. L., Kwan, A. J., Surratt, J. D., Chan, A. W. H., Chhabra, P. S., & Sorooshian, A. (2008). Secondary organic aerosol (SOA) formation from reaction of isoprene with nitrate radicals (NO_3). *Atmospheric Chemistry and Physics*, *8*(14), 4117–4149. https://doi.org/10.5194/acp-8-4117-2008

Oderbolz, D. C., Aksoyoglu, S., Keller, J., Barmpadimos, I., Steinbrecher, R., & Skjøth, C. A. (2013). A comprehensive emission inventory of biogenic volatile organic compounds in Europe: Improved seasonality and land-cover. *Atmospheric Chemistry and Physics*, *13*(4), 1689–1712. https://doi.org/10.5194/acp-13-1689-2013

Odum, J. R., Hoffmann, T., Bowman, F., Collins, D., Flagan, R. C., & Seinfeld, J. H. (1996). Gas/particle partitioning and secondary organic aerosol yields. *Environmental Science & Technology*, *30*(8), 2580–2585. https://doi.org/10.1021/es950943+

Pankow, J. F. (1994). An absorption model of gas/particle partitioning of organic compounds in the atmosphere. *Atmospheric Environment*, *28*(2), 185–188. https://doi.org/10.1016/1352-2310(94)90093-0

Popkin, G. (2019). The forest question. *Nature*, *565*, 280–282. https://doi.org/10.1038/d41586-019-00122-z

Poulain, L., Birmili, W., Canonaco, F., Crippa, M., Wu, Z. J., Nordmann, S., et al. (2014). Chemical mass balance of 300 degrees C non-volatile particles at the tropospheric research site Melpitz, Germany. *Atmospheric Chemistry and Physics*, *14*, 10145–10162. https://doi.org/10.5194/acp-14-10145-2014

Poulain, L., Spindler, G., Birmili, W., Plass-Dülmer, C., Wiedensohler, A., & Herrmann, H. (2011). Seasonal and diurnal variations of particulate nitrate and organic matter at the IfT research station Melpitz. *Atmospheric Chemistry and Physics*, *11*, 12579–12599. https://doi.org/10.5194/acp-11-12579-2011

Pouliot, G., Denier van der Gon, H., Kuenen, J., Makar, P., Zhang, J., & Moran, M. (2015). Analysis of the emission inventories and model-ready emission datasets of Europe and North America for phase 2 of the AQMEII project. *Atmospheric Environment*, *115*, 345–360. https://doi.org/10.1016/j.atmosenv.2014.10.061

Riccobono, F., Schobesberger, S., Scott, C. E., Dommen, J., Ortega, I. K., & Rondo, L. (2014). Oxidation products of biogenic emissions contribute to nucleation of atmospheric particles. *Science*, *344*(6185), 717–721. https://doi.org/10.1126/science.1243527

Richters, S., Herrmann, H., & Berndt, T. (2016). Highly oxidized RO_2 radicals and consecutive products from the ozonolysis of three sesquiterpenes. *Environmental Science & Technology*, *50*(5), 2354–2362. https://doi.org/10.1021/acs.est.5b05321

Schättler, U., Doms, G., & Schraff, C. (2018). *A description of the nonhydrostatic regional COSMO-model partVII: User's guide*. Deutscher Wetterdinst. Retrieved from http://www.cosmo-model.org/

Schell, B., Ackermann, I. J., Hass, H., Binkowski, F. S., & Ebel, A. (2001). Modeling the formation of secondary organic aerosol within a comprehensive air quality model system. *Journal of Geophysical Research: Atmospheres*, *106*(D22), 28275–28293. https://doi.org/10.1029/2001JD000384

Schlünzen, K. H., & Katzfey, J. J. (2003). Relevance of sub-grid-scale land-use effects for mesoscale models. *Tellus*, *55*(3), 232–246. https://doi.org/10.1034/j.1600-0870.2003.00017.x

Schlünzen, K. H., & Pahl, S. (1992). Modification of dry deposition in a developing sea-breeze circulation-A numerical case study. *Atmospheric Environment Part A. General Topics*, *26*(1), 51–61. https://doi.org/10.1016/0960-1686(92)90260-R

Schneider, C., Pelzer, M., Toenges-Schuller, N., Nacken, M., & Niederau, A. (2016). *ArcGIS basierte Lösung zur detaillierten, deutschlandweiten Verteilung (Gridding) nationaler Emissionsjahreswerte auf Basis des Inventars zur Emissionsberichterstattung (TEXTE 71/2016, Forschungskennzahl 3712 63 240 2 UBA-FB-002360)*. Dessau-Roßlau.

Schubert, S., & Grossman-Clarke, S. (2013). The Influence of green areas and roof albedos on air temperatures during Extreme Heat Events in Berlin, Germany. *Meteorologische Zeitschrift*, *22*(2), 131–143. https://doi.org/10.1127/0941-2948/2013/0393

Schultz, M. G., Stadtler, S., Schröder, S., Taraborrelli, D., Franco, B., Krefting, J., et al. (2018). The chemistry–climate model ECHAM6.3-HAM2.3-MOZ1.0. *Geoscientific Model Development*, *11*(5), 1695–1723. https://doi.org/10.5194/gmd-11-1695-2018

Seneviratne, S. I., Corti, T., Davin, E. L., Hirschi, M., Jaeger, E. B., Lehner, I., et al. (2010). Investigating soil moisture–climate interactions in a changing climate: A review. *Earth-Science Reviews*, *99*(3–4), 125–161. https://doi.org/10.1016/j.earscirev.2010.02.004

Silva, J., Ribeiro, C., Guedes, R., Rua, M.-C., & Ulrich, F. (2007). *Roughness length classification of CORINE Land Cover classes*. Paper presented at Proceedings of European Wind Energy Conference 2007, Milan, Italy.

Simpson, D., Benedictow, A., Berge, H., Bergström, R., Emberson, L. D., Fagerli, H., et al. (2012). The EMEP MSC-W chemical transport model – Technical description. *Atmospheric Chemistry and Physics*, *12*(16), 7825–7865. https://doi.org/10.5194/acp-12-7825-2012

Solazzo, E., Bianconi, R., Pirovano, G., Matthias, V., Vautard, R., Moran, M. D., et al. (2012). Operational model evaluation for particulate matter in Europe and North America in the context of AQMEII. *Atmospheric Environment*, *53*, 75–92. https://doi.org/10.1016/j.atmosenv.2012.02.045

Solazzo, E., Bianconi, R., Vautard, R., Appel, K. W., Moran, M. D., Hogrefe, C., et al. (2012). Ensemble modelling of surface level ozone in Europe and North America in the context of AQMEII. *Atmospheric Environment*, *53*, 60–74. https://doi.org/10.1016/j.atmosenv.2012.01.003

Spindler, G., Gnauk, T., Grüner, A., Iinuma, Y., Müller, K., Scheinhardt, S., et al. (2012). Size-segregated characterization of PM_{10} at the EMEP site Melpitz (Germany) using a five-stage impactor: A six year study. *Jornal of Atmospheric Chemistry*, *69*, 127–157. https://doi.org/10.1007/s10874-012-9233-6

Spindler, G., Grüner, A., Müller, K., Schlimper, S., & Herrmann, H. (2013). Long-term size-segregated particle (PM_{10}, $PM_{2.5}$, PM_1) characterization study at Melpitz—Influence of air mass inflow, weather conditions and season. *Journal of Atmospheric Chemistry*, *70*(2), 165–195. https://doi.org/10.1007/s10874-013-9263-8

Steinbrecher, R., Smiatek, G., Köble, R., Seufert, G., Theloke, J., & Hauff, K. (2009). Intra- and inter-annual variability of VOC emissions from natural and semi-natural vegetation in Europe and neighbouring countries. *Atmospheric Environment*, *43*(7), 1380–1391. https://doi.org/10.1016/j.atmosenv.2008.09.072

Stockwell, W. R., Kirchner, F., Kuhn, M., & Seefeld, S. (1997). A new mechanism for regional atmospheric chemistry modeling. *Journal of Geophysical Research: Atmospheres*, *102*(D22), 25847–25879. https://doi.org/10.1029/97JD00849

Stohl, A., Williams, E., Wotawa, G., & Kromp-Kolb, H. (1996). A European inventory of soil nitric oxide emissions and the effect of these emissions on the photochemical formation of ozone. *Atmospheric Environment*, *30*(22), 3741–3755. https://doi.org/10.1016/1352-2310(96)00104-5

Supuka, J., Berta, F., & Chladná, A. (1997). The Influence of the urban environment on the composition of terpenes in the needles of Black Pine (Pinus nigra Arnold). *Trees*, *11*(3), 176–182. https://doi.org/10.1007/PL00009666

von Schneidemesser, E., Monks, P. S., Allan, J. D., Bruhwiler, L., Forster, P., Fowler, D., et al. (2015). Chemistry and the Linkages between air quality and climate change. *Chemical Reviews*, *115*(10), 3856–3897. https://doi.org/10.1021/acs.chemrev.5b00089

Williams, E. J., Guenther, A., & Fehsenfeldi, F. C. (1992). An inventory of nitric oxide emissions from soils in the United States. *Journal of Geophysical Research: Atmospheres*, *97*(D7), 7511–7519. https://doi.org/10.1029/92JD00412

Wolke, R., & Knoth, O. (2000). Implicit-explicit Runge-Kutta methods applied to atmospheric chemistry-transport modelling. *Environmental Modelling & Software*, *15*(6–7), 711–719. https://doi.org/10.1016/S1364-8152(00)00034-7

Wolke, R., Knoth, O., Hellmuth, O., Schröder, W., & Renner, E. (2004). The parallel model system LM-MUSCAT for chemistry-transport simulations: Coupling scheme, parallelization and application. In G. R. Joubert, W. E. Nagel, F. J. Peters, & W. V. Walter (Eds.), *Parallel computing: Software Technology, Algorithms, Architectures, and Applications* (Vol. 13, pp. 363–369). Elsevier.

Wolke, R., Schröder, W., Schrödner, R., & Renner, E. (2012). Influence of grid resolution and meteorological forcing on simulated European air quality: A sensitivity study with the modeling system COSMO–MUSCAT. *Atmospheric Environment*, *53*, 110–130. https://doi.org/10.1016/j.atmosenv.2012.02.085

Zhang, L., Brook, J. R., & Vet, R. (2003). A revised parameterization for gaseous dry deposition in air-quality models. *Atmospheric Chemistry and Physics*, *3*, 2067–2082. https://doi.org/10.5194/acp-3-2067-2003

References From the Supporting Information

Barsanti, K. C., Carlton, A. G., & Chung, S. H. (2013). Analyzing experimental data and model parameters: Implications for predictions of SOA using chemical transport models. *Atmospheric Chemistry and Physics*, *13*(23), 12073–12088. https://doi.org/10.5194/acp-13-12073-2013

Bingöl, F. (2019). A simplified method on estimation of forest roughness by use of aerial LIDAR data. *Energy Science & Engineering*, *7*(6), 3274–3282. https://doi.org/10.1002/ese3.496

Blande, J. D., Holopainen, J. K., & Niinemets, Ü. (2014). Plant volatiles in polluted atmospheres: Stress responses and signal degradation: Plant volatiles in a polluted atmosphere. *Plant, Cell and Environment*, *37*(8), 1892–1904. https://doi.org/10.1111/pce.12352

Calfapietra, C., Peñuelas, J., & Niinemets, Ü. (2015). Urban plant physiology: Adaptation-mitigation strategies under permanent stress. *Trends in Plant Science*, *20*(2), 72–75. https://doi.org/10.1016/j.tplants.2014.11.001

Carlton, A. G., Bhave, P. V., Napelenok, S. L., Edney, E. O., Sarwar, G., Pinder, R. W., et al. (2010). Model representation of secondary organic aerosol in CMAQv4.7. *Environmental Science & Technology*, *44*(22), 8553–8560. https://doi.org/10.1021/es100636q

Carlton, A. G., Wiedinmyer, C., & Kroll, J. H. (2009). A review of Secondary Organic Aerosol (SOA) formation from isoprene. *Atmospheric Chemistry and Physics*, *9*, 4987–5005. https://doi.org/10.5194/acp-9-4987-2009

Chan, A. W. H., Chan, M. N., Surratt, J. D., Chhabra, P. S., Loza, C. L., Crounse, J. D., et al. (2010). Role of aldehyde chemistry and NO_x concentrations in secondary organic aerosol formation. *Atmospheric Chemistry and Physics*, *10*(15), 7169–7188. https://doi.org/10.5194/acp-10-7169-2010

Dai, Y., Dickinson, R. E., & Wang, Y.-P. (2004). A two-big-leaf model for canopy temperature, photosynthesis, and stomatal conductance. *Journal of Climate*, *17*(12), 2281–2299. https://doi.org/10.1175/1520-0442(2004)017<2281:ATMFCT>2.0.CO;2

De Pury, D. G. G., & Farquhar, G. D. (1997). Simple scaling of photosynthesis from leaves to canopies without the errors of big-leaf models. *Plant, Cell and Environment*, *20*(5), 537–557. https://doi.org/10.1111/j.1365-3040.1997.00094.x

Dommen, J., Metzger, A., Duplissy, J., Kalberer, M., Alfarra, M. R., Gascho, A., et al. (2006). Laboratory observation of oligomers in the aerosol from isoprene/NO_x photooxidation. *Geophysical Research Letters*, *33*, L13805. https://doi.org/10.1029/2006GL026523

Farina, S. C., Adams, P. J., & Pandis, S. N. (2010). Modeling global secondary organic aerosol formation and processing with the volatility basis set: Implications for anthropogenic secondary organic aerosol. *Journal of Geophysical Research*, *115*, D09202. https://doi.org/10.1029/2009JD013046

Feng, J., Liu, H., Wang, L., Du, Q., & Shi, L. (2012). Seasonal and inter-annual variation of surface roughness length and bulk transfer coefficients in a semiarid area. *Science China Earth Sciences*, *55*(2), 254–261. https://doi.org/10.1007/s11430-011-4258-2

Floors, R., Badger, M., Troen, I., Grogan, K., & Permien, F.-H. (2021). Satellite-based estimation of roughness lengths and displacement heights for wind resource modelling. *Wind Energy Science*, *6*(6), 1379–1400. https://doi.org/10.5194/wes-6-1379-2021

Fuentes, J. D., Gu, L., Lerdau, M., Atkinson, R., Baldocchi, D., Bottenheim, J. W., et al. (2000). Biogenic hydrocarbons in the atmospheric boundary layer: A review. *Bulletin of the American Meteorological Society*, *81*(7), 1537–1575. https://doi.org/10.1175/1520-0477(2000)081<1537:BHITAB>2.3.CO;2

Gatzsche, K. (2019). *Investigation of gasSOA formation by parcel and 3-D modeling* (Doctoral dissertation). Universität Leipzig. Retrieved from https://nbn-resolving.org/urn:nbn:de:bsz:15-qucosa2-338802

Grote, R., Sharma, M., Ghirardo, A., & Schnitzler, J.-P. (2019). A new modeling approach for estimating abiotic and biotic stress-induced de novo emissions of biogenic volatile organic compounds from plants. *Frontiers in Forests and Global Change*, *2*, 26. https://doi.org/10.3389/ffgc.2019.00026

Guenther, A. B., Karl, T., Harley, P., Wiedinmyer, C., Palmer, P. I., Geron, C. (2006). Estimates of global terrestrial isoprene emissions using MEGAN (model of emissions of gases and aerosols from nature). *Atmospheric Chemistry and Physics*, *6*(11), 3181–3210. https://doi.org/10.5194/acp-6-3181-2006

Heisler, G. M. (1986). Effects of individual trees on the solar radiation climate of small buildings. *Urban Ecology*, *9*(3), 337–359. https://doi.org/10.1016/0304-4009(86)90008-2

Henze, D. K., & Seinfeld, J. H. (2006). Global secondary organic aerosol from isoprene oxidation. *Geophysical Research Letters*, *33*, L09812. https://doi.org/10.1029/2006GL025976

Holopainen, J. K., & Gershenzon, J. (2010). Multiple stress factors and the emission of plant VOCs. *Trends in Plant Science*, *15*(3), 176–184. https://doi.org/10.1016/j.tplants.2010.01.006

Keenan, T. F., Grote, R., & Sabaté, S. (2011). Overlooking the canopy: The importance of canopy structure in scaling isoprenoid emissions from the leaf to the landscape. *Ecological Modelling*, *222*(3), 737–747. https://doi.org/10.1016/j.ecolmodel.2010.11.004

Kesselmeier, J., & Staudt, M. (1999). Biogenic volatile organic compounds (VOC): An overview on emission, physiology and ecology. *Journal of Atmospheric Chemistry*, *33*, 23–88. https://doi.org/10.1023/A:1006127516791

Kopaczyk, J. M., Warguła, J., & Jelonek, T. (2020). The variability of terpenes in conifers under developmental and environmental stimuli. *Environmental and Experimental Botany*, *180*, 104197. https://doi.org/10.1016/j.envexpbot.2020.104197

Komenda, M., & Koppmann, R. (2002). Monoterpene emissions from Scots pine (*Pinus sylvestris*): Field studies of emission rate variabilities. *Journal of Geophysical Research*, *107*(D13), ACH1-1–ACH1-13. https://doi.org/10.1029/2001JD000691

Krayenhoff, E. S., Jiang, T., Christen, A., Martilli, A., Oke, T. R., Bailey, B. N., et al. (2020). A multi-layer urban canopy meteorological model with trees (BEP-Tree): Street tree impacts on pedestrian-level climate. *Urban Climate*, *32*, 100590. https://doi.org/10.1016/j.uclim.2020.100590

Kroll, J. H., Ng, N. L., Murphy, S. M., Flagan, R. C., & Seinfeld, J. H. (2005). Secondary organic aerosol formation from isoprene photooxidation under high-NO_x conditions: SOA formation from isoprene oxidation. *Geophysical Research Letters*, *32*, L18808. https://doi.org/10.1029/2005GL023637

Lane, T. E., Donahue, N. M., & Pandis, S. N. (2008). Simulating secondary organic aerosol formation using the volatility basis-set approach in a chemical transport model. *Atmospheric Environment*, *42*(32), 7439–7451. https://doi.org/10.1016/j.atmosenv.2008.06.026

Mazza, G., Agnelli, A. E., & Lagomarsino, A. (2021). The effect of tree species composition on soil C and N pools and greenhouse gas fluxes in a Mediterranean reforestation. *Journal of Soil Science and Plant Nutrition*, *21*(2), 1339–1352. https://doi.org/10.1007/s42729-021-00444-w

Meili, N., Manoli, G., Burlando, P., Carmeliet, J., Chow, W. T. L., Coutts, A. M., et al. (2021). Tree effects on urban microclimate: Diurnal, seasonal, and climatic temperature differences explained by separating radiation, evapotranspiration, and roughness effects. *Urban Forestry and Urban Greening*, *58*, 126970. https://doi.org/10.1016/j.ufug.2020.126970

Merikanto, J., Spracklen, D. V., Mann, G. W., Pickering, S. J., & Carslaw, K. S. (2009). Impact of nucleation on global CCN. *Atmospheric Chemistry and Physics*, *9*, 8601–8616. https://doi.org/10.5194/acp-9-8601-2009

Miao, Y., Li, J., Miao, S., Che, H., Wang, Y., Zhang, X., et al. (2019). Interaction between planetary boundary layer and PM2.5 pollution in megacities in China: A review. *Current Pollution Reports*, *5*(4), 261–271. https://doi.org/10.1007/s40726-019-00124-5

Murphy, B. N., & Pandis, S. N. (2009). Simulating the formation of semivolatile primary and secondary organic aerosol in a regional chemical transport model. *Environmental Science & Technology*, *43*(13), 4722–4728. https://doi.org/10.1021/es803168a

Müller, J.-F., Stavrakou, T., Wallens, S., De Smedt, I., Van Roozendael, M., Potosnak, M. J., et al. (2008). Global isoprene emissions estimated using MEGAN, ECMWF analyses and a detailed canopy environment model. *Atmospheric Chemistry and Physics*, *8*(5), 1329–1341. https://doi.org/10.5194/acp-8-1329-2008

Müller, J.-F., Stavrakou, T., & Peeters, J. (2019). Chemistry and deposition in the model of atmospheric composition at global and regional scales using inversion techniques for Trace gas emissions (MAGRITTE v1.1)—Part 1: Chemical mechanism. *Geoscientific Model Development*, *12*(6), 2307–2356. https://doi.org/10.5194/gmd-12-2307-2019

Niinemets, Ü. (2009). Mild versus severe stress and BVOCs: Thresholds, priming and consequences. *Trends in Plant Science*, *15*(3), 145–153. https://doi.org/10.1016/j.tplants.2009.11.008

Niinemets, Ü., Arneth, A., Kuhn, U., Monson, R. K., Peñuelas, J., & Staudt, M. (2010). The emission factor of volatile isoprenoids: Stress, acclimation, and developmental responses. *Biogeosciences*, *7*, 2203–2223. https://doi.org/10.5194/bgd-7-1529-2010

Pun, B. K., Wu, S.-Y., Seigneur, C., Seinfeld, J. H., Griffin, R. J., & Pandis, S. N. (2003). Uncertainties in modeling secondary organic aerosols: Three-dimensional modeling studies in Nashville/western Tennessee. *Environmental Science & Technology*, *37*(16), 3647–3661. https://doi.org/10.1021/es0341541

Pye, H. O. T., Chan, A. W. H., Barkley, M. P., & Seinfeld, J. H. (2010). Global modeling of organic aerosol: The importance of reactive nitrogen (NO_x and NO_3). *Atmospheric Chemistry and Physics*, *10*(22), 11261–11276. https://doi.org/10.5194/acp-10-11261-2010

Riipinen, I., Pierce, J. R., Yli-Juuti, T., Nieminen, T., Häkkinen, S., Ehn, M., et al. (2011). Organic condensation: A vital link connecting aerosol formation to cloud condensation nuclei (CCN) concentrations. *Atmospheric Chemistry and Physics*, *11*(8), 3865–3878. https://doi.org/10.5194/acp-11-3865-2011

Schobesberger, S., Franchin, A., Bianchi, F., Rondo, L., Duplissy, J., Kürten, A., et al. (2015). On the composition of ammonia–sulfuric-acid ion clusters during aerosol particle formation. *Atmospheric Chemistry and Physics*, *15*(1), 55–78. https://doi.org/10.5194/acp-15-55-2015

Staudt, M., Bertin, N., Frenzel, B., & Seufert, G. (2000). Seasonal variation in amount and composition of monoterpenes emitted by young Pinus pinea trees—Implications for emission modeling. *Journal of Atmospheric Chemistry*, *35*, 77–99. https://doi.org/10.1023/A:1006233010748

Tsimpidi, A. P., Karydis, V. A., Zavala, M., Lei, W., Molina, L., Ulbrich, I. M., et al. (2010). Evaluation of the volatility basis-set approach for the simulation of organic aerosol formation in the Mexico City metropolitan area. *Atmospheric Chemistry and Physics*, *10*, 525–546. https://doi.org/10.5194/acp-10-525-2010

Vatani, L., Hosseini, S. M., Raeini Sarjaz, M., Alavi, S. J., Shamsi, S. S., & Zohd Ghodsi, M. J. (2019). Effect of tree species on albedo in Iranian temperate forests: Comparing conifers and broadleaf trees in two seasons. *Journal of Solar Energy Research*, *4*(3), 188–199. https://doi.org/10.22059/jser.2019.289156.1128

Wang, H., Wu, Q., Liu, H., Wang, Y., Cheng, H., Wang, R., et al. (2018). Sensitivity of biogenic volatile organic compound emissions to leaf area index and land cover in Beijing. *Atmospheric Chemistry and Physics*, *18*(13), 9583–9596. https://doi.org/10.5194/acp-18-9583-2018

Yan, C., Nie, W., Vogel, A. L., Dada, L., Lehtipalo, K., Stolzenburg, D., et al. (2020). Size-dependent influence of NO_x on the growth rates of organic aerosol particles. *Science Advances*, *6*(22), eaay4945. https://doi.org/10.1126/sciadv.aay4945

Zhang, M., Zhao, C., Yang, Y., Du, Q., Shen, Y., Lin, S., et al. (2021). Modeling sensitivities of BVOCs to different versions of MEGAN emission schemes in WRF-Chem (v3.6) and its impacts over eastern China. *Geoscientific Model Development*, *14*(10), 6155–6175. https://doi.org/10.5194/gmd-14-6155-2021

Zhang, Y., Huang, J.-P., Henze, D. K., & Seinfeld, J. H. (2007). Role of isoprene in secondary organic aerosol formation on a regional scale. *Journal of Geophysical Research*, *112*, D20207. https://doi.org/10.1029/2007JD008675

Zhou, Y., Sun, X., Ju, W., Wen, X., & Guan, D. (2012). Seasonal, diurnal and wind-direction-dependent variations of the aerodynamic roughness length in two typical forest ecosystems of China. *Terrestrial, Atmospheric and Oceanic Sciences*, *23*(2), 181. https://doi.org/10.3319/TAO.2011.10.06.01